Chemistry–A European Journal

Research Article
doi.org/10.1002/chem.202400871

Chemistry Europe
European Chemical
Societies Publishing

www.chemeurj.org

Identification of Potential Drug Targets of Calix[4]arene by Reverse Docking

Giulia Giugliano,[a] Margherita Gajo,[a] Tainah Dorina Marforio,[a] Francesco Zerbetto,[a] Edoardo Jun Mattioli,*[a] and Matteo Calvaresi*[a]

Calixarenes are displaying great potential for the development of new drug delivery systems, diagnostic imaging, biosensing devices and inhibitors of biological processes. In particular, calixarene derivatives are able to interact with many different enzymes and function as inhibitors. By screening of the potential drug target database (PDTD) with a reverse docking procedure, we identify and discuss a selection of 100 proteins that interact strongly with calix[4]arene. We also discover that leucine (23.5%), isoleucine (11.3%), phenylalanines (11.3%) and valine (9.5%) are the most frequent binding residues followed by hydrophobic cysteines and methionines and aromatic histidines, tyrosines and tryptophanes. Top binders are peroxisome proliferator-activated receptors that already are targeted by commercial drugs, demonstrating the practical interest in calix[4]arene. Nuclear receptors, potassium channel, several carrier proteins, a variety of cancer-related proteins and viral proteins are prominent in the list. It is concluded that calix[4]arene, which is characterized by facile access, well-defined conformational characteristics, and ease of functionalization at both the lower and higher rims, could be a potential lead compound for the development of enzyme inhibitors and theranostic platforms.

Introduction

Calix[n]arenes (with n commonly 4, 5, 6 or 8) are macrocycles comprising phenolic units linked by methylene groups at positions 2 and 6. They are characterized by a bowl-like shape, with cavities of different sizes (depending on n). Calixarenes represent one of the most investigated molecular scaffolds in supramolecular chemistry.

The application of calixarenes in medicine is a burgeoning field with promising implications for drug delivery, diagnostics, and therapeutics.[1–5] The cyclic framework and the hydrophobic cavities of calixarenes make them particularly attractive for various medical applications that include:[1–6]

(1) Delivery Systems. Calixarenes serve as excellent hosts for encapsulating guest molecules, a property that has been harnessed for drug delivery applications.[7] By encapsulating therapeutic agents within their cavities, calixarenes enhance their stability and solubility.[7] In addition, the drug-encapsulation allows controlled release at specific sites, minimizing side effects and optimizing therapeutic efficacy. For example, in the field of oncology, the ability of calixarenes to selectively encapsulate anti-cancer drugs[8,9] enables their delivery directly to tumor cells, reducing the impact on healthy tissues.

(2) Diagnostic Imaging. Calixarenes are being explored for their application in diagnostic imaging techniques. Their structure can be tailored to incorporate imaging agents such as contrast agents for magnetic resonance imaging (MRI),[10] radionuclides for positron emission tomography (PET) or luminescent agents.[11–15] This allows to develop more efficient and precise imaging probes for early disease detection and monitoring.[16]

(3) Biosensors. Calixarenes are used in biosensors design for detecting specific biomolecules. Functionalized calixarenes can selectively bind to target analytes, leading to measurable changes in various signal transduction methods.[13] This application is valuable for the early detection of diseases and monitoring of biomarkers in real-time.

(4) Inhibitors. Calixarenes exhibit significant potential as inhibitors of various biological processes, owing to their ability to selectively interact with biomolecules. The inhibitory properties of calixarenes have been explored in different contexts, ranging from the modulation of protein-protein interactions to enzyme inhibition.[17]

On the one side, working as supramolecular hosts, calixarenes can be functionalized to selectively bind to protein surfaces.[6,17–31] This property has been explored in the context of protein-protein interactions,[6,17–31] where calixarenes act as modulators that interfere with the binding interfaces of interacting proteins.[6,17–31] Such inhibition can have implications in the regulation of signaling pathways and cellular processes.[6,17–31] Calixarenes were modified to interact with viral proteins, hindering the attachment and entry of viruses into host cells.[24] This potential antiviral activity could be a potential winner for the development of new strategies in the fight against viral diseases.[24,32,33]

On the other side, working as guests, calixarenes were studied also for their ability to inhibit specific enzymes. The

Chem. Eur. J. 2024, 30, e202400871 (1 of 20)

© 2024 Wiley-VCH GmbH

Chemistry–A European Journal

Research Article
doi.org/10.1002/chem.202400871

Chemistry Europe
European Chemical
Societies Publishing

versatility of calixarenes in terms of structural modifications and functionalization makes them valuable tools for designing targeted inhibitors for specific enzymes. In this case, the smallest calix[4]arene represents the ideal scaffold to develop inhibitors, due to its rigidity that strongly reduces the entropic penalty typical of every binding process. Calixarene derivatives are efficient inhibitors of alkaline phosphatase,[34–36] ion channels,[37] histone deacetylase,[38] galectin-1,[39,40] glutathione-S- transferase,[41,42] tyrosine phosphatase,[43–46] HIV-1 integrase,[47,48] HIV protease,[49] protein disulfide isomerase,[50] AXL tyrosine kinase receptor,[51] HIV-1 nucleocapsid protein,[52] α-mannosidase,[53] bromelain and polyphenol oxidase,[54] and carbonic anhydrase.[55]

Over the last twenty years, a substantial amount of work was carried out to study the interaction of calixarene derivatives with biomolecules, in particular to identify their interactions with druggable proteins. Virtual screening using molecular docking and experimental screening of a library of calixarene derivatives were the two main approaches used to find calixarene derivatives that can bind to a known biomolecular target selectively.

In this paper we develop a rational approach, based on reverse docking, to design protein inhibitors using the calix[4]arene as molecular scaffold. In practice, we used calix[4]arene as a bait to fish out specific proteins from a database of druggable proteins, able to interact with it.

Results and Discussion

Screening of the potential drug target database (PDTD) with a docking procedure (reverse docking) can reveal potential calix[4]arene binding targets of interest for biological and pharmacological activity. Calix[4]arene is of particular interest because of its facile access, well-defined conformational characteristics (Figure 1A), and ease of functionalization at both the lower and higher rims for lead optimization.[56] Four different conformations can be identified for calix[4]arene: cone, partial cone, 1,3-alternate, and 1,2-alternate. Initially, DFT calculations evaluated quantitatively the relative stabilities of the four conformers in physiological environment (water). The result (Figure 1B) is cone (most stable) > partial-cone (+ 5.9 kcal mol^{-1}) > 1,2-alternate (+9.1 kcal mol^{-1}) > 1,3-alternate (+ 10.7 kcal mol^{-1}).

Due to the intramolecular hydrogen-bonding involving the four OH groups, calix[4]arene preferentially adopts the cone conformation. Upon binding to a protein, the preferred conformation of calix[4]arene may change. In the reverse docking calculations, we evaluated every time the binding of a protein with all the four possible conformations of calix[4]arene. The energy penalty necessary to vary the conformation of the calix[4]arene from the most stable cone conformation was included in the analysis.

The calculations were carried out for the entire database. Proteins ranking in the top 100 (Table 1) are discussed and analyzed since they can be considered as the most probable hits. The analysis suggests that the most compact and energetically favored structure is the cone conformer.

Peroxisome proliferator-activated receptor alpha. The first position of the ranking is occupied by the peroxisome proliferator-activated receptor alpha (PPAR-α), a nuclear receptor protein functioning as a transcription factor (Figure 2). It is regulated by free fatty acids and is a major regulator of lipid metabolism in the liver. Fatty acids like stearic and palmitic
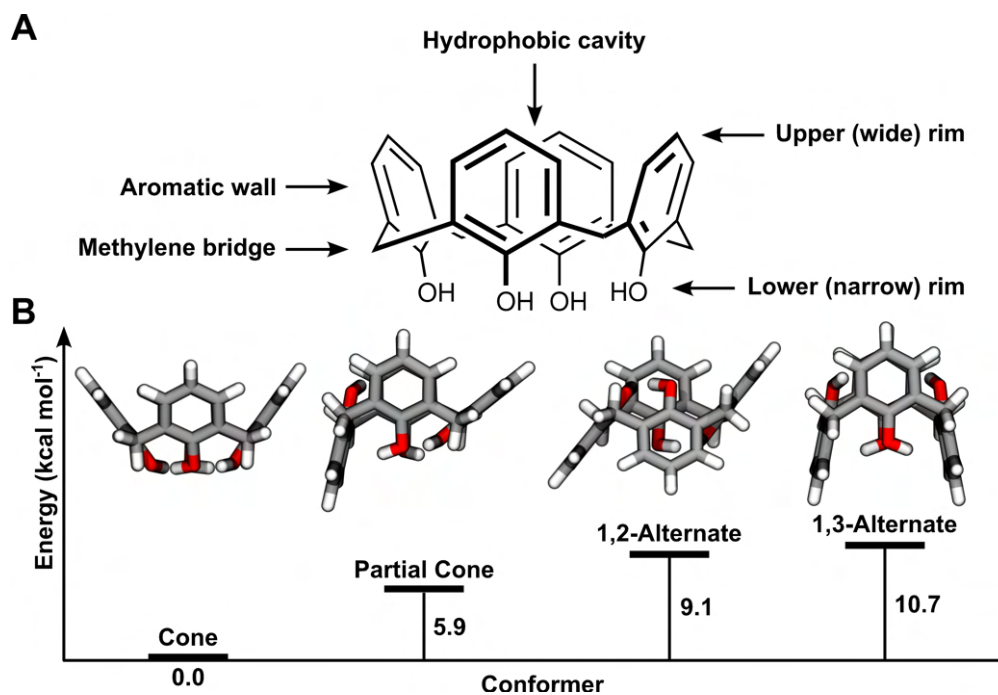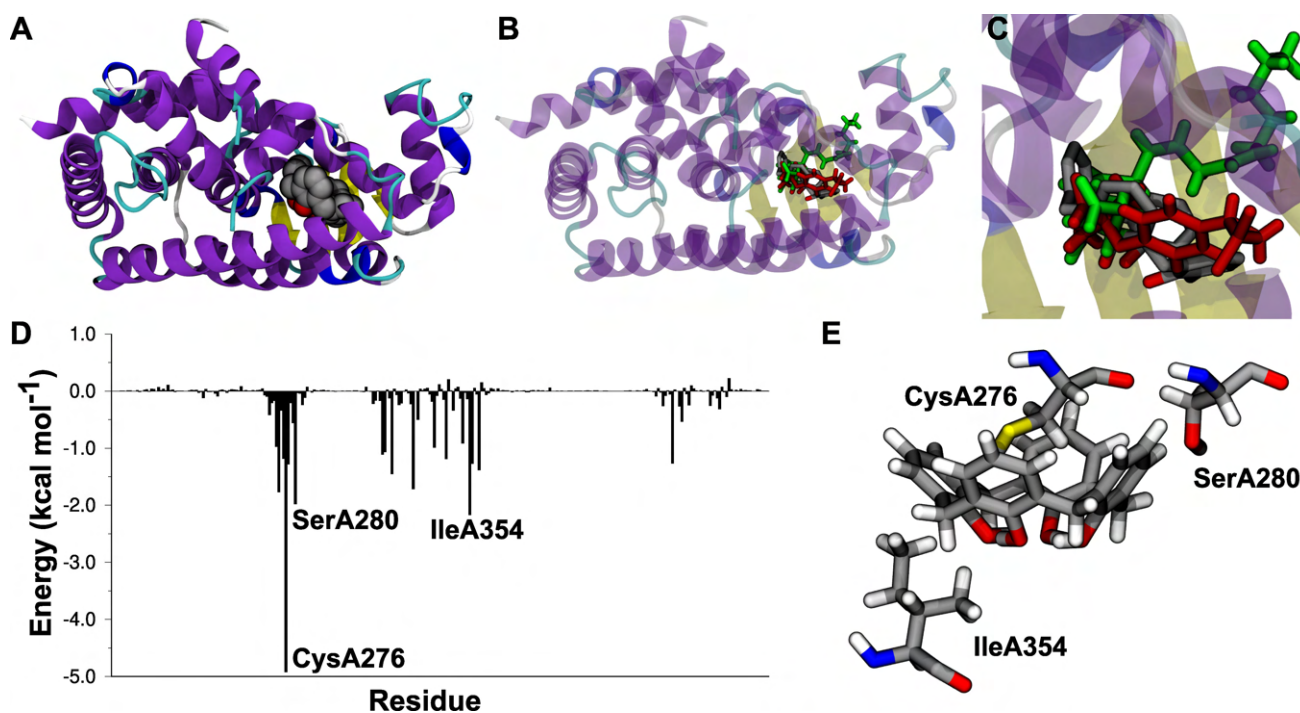

Figure 1. A. Structure of calix[4]arene in cone conformation. B. Calculated relative stabilities of the four main conformations of calix[4]arene in water.

Chemistry–A European Journal

Research Article
doi.org/10.1002/chem.202400871

Chemistry Europe
European Chemical
Societies Publishing

Table 1. Top 100 Protein Target candidates for binding calix[4]arene as ranked by the reverse docking procedure. $\Delta E_{binding}$ are reported in kcal mol⁻¹.

Rank	PDB	Protein name	Conformer	Affinity (kcal mol⁻¹)	Rank	PDB	Protein name	Conformer	Affinity (kcal mol⁻¹)
1	1K7L	Peroxisome proliferator-activated receptor alpha	Cone	−61.9	51	1XKK	EGFR2 kinase-domain	Cone	−42.1
2	1FM6	Peroxisome proliferator-activated receptor gamma	Cone	−59.1	52	1DMH	Catechol 1,2-dioxygenase	Cone	−42.1
3	1PHG	Camphor 5-monooxygenase	Cone	−57.3	53	1BOZ	Dihydrofolate reductase	Cone	−42.0
4	1I19	Cholesterol oxidase	Cone	−55.7	54	1W6K	Lanosterol synthase	Cone	−41.8
5	1QKM	Estrogen receptor beta	Cone	−55.0	55	1AL8	Short chain alpha-hydroxy acid oxidase	Cone	−41.7
6	1JVM	pH-gated potassium channel KcsA	Cone	−53.5	56	1HT8	Cyclooxygenase-1	1,2-Alternate	−41.7
7	1PCG	Estrogen receptor alpha	Cone	−52.7	57	1HTE	HIV-1 protease	Cone	−41.4
8	1VE9	D-amino-acid oxidase	Cone	−51.2	58	2IFB	Fatty acid-binding protein, intestinal	Cone	−41.3
9	2F9Q	Cytochrome P450 2D6	Cone	−51.2	59	2BX8	Albumin	Cone	−41.3
10	1Y0S	Peroxisome proliferator-activated receptor delta	Cone	−51.1	60	1ACM	Aspartate carbamoyltransferase catalytic subunit	Cone	−41.2
11	1E3K	Progesterone receptor	Cone	−50.5	61	1WKD	Queuine tRNA-ribosyltransferase	Cone	−40.8
12	1E3G	Androgen receptor	Cone	−50.1	62	1ILH	Pregnane X receptor	Cone	−40.7
13	8CAT	Catalase	Cone	−49.9	63	1DR1	Dihydrofolate reductase	Cone	−40.7
14	2MBR	UDP-N-Acetylenolpyruvoylglucosamine reductase	Cone	−49.7	64	1R0P	Hepatocyte growth factor receptor	Cone	−40.7
15	1XNX	Androstane receptor	Cone	−49.5	65	2VAB	H-2 class I histocompatibility antigen, K–B alpha chain	Cone	−40.6
16	1P93	Glucocorticoid receptor	Cone	−49.5	66	1OYA	NADPH dehydrogenase 1	Cone	−40.6
17	1IJH	Cholesterol oxidase	Cone	−49.5	67	1D2V	Myeloperoxidase	1,2-Alternate	−40.5
18	1UHL	Retinoic acid receptor RXR-beta	Cone	−49.3	68	1DKF	Retinoic acid receptor RXR-alpha	Cone	−40.5
19	1D8R	Dihydrofolate reductase	Cone	−48.6	69	1OGS	Acid beta-glucosidase	Cone	−40.1
20	1BIF	6-phosphofructo-2-kinase/fructose-2,6-bisphosphatase 4	Cone	−48.4	70	1Y5M	7-oxosteroid reductase	Cone	−40.0
21	1JS3	Aromatic-L-amino-acid decarboxylase	Cone	−47.9	71	1VJT	Alpha-glucosidase, putative	Cone	−40.0
22	1ZHY	Oxysterol-binding protein-related protein 4	Cone	−47.8	72	1CW2	Tryptophan synthase alpha chain	Cone	−39.8
23	1K4W	Nuclear receptor ROR-beta	Cone	−47.8	73	1E6U	GDP–L-fucose synthase	Cone	−39.8
24	1PQ2	Cytochrome P450 2 C8	Cone	−47.7	74	2A3L	AMP deaminase	Cone	−39.7
25	1OG5	Cytochrome P450 CYP2 C9	Cone	−47.5	75	1PYY	Penicillin-binding protein 2X	Cone	−39.6
26	1DF7	Dihydrofolate reductase	Cone	−46.7	76	1BBP	Bilin-binding protein	Cone	−39.4
27	1BVY	Cytochrome P450 102A1	1,2-Alternate	−46.5	77	2AC3	MAP kinase-interacting serine/threonine-protein kinase 2	Cone	−39.4
28	1ADB	Alcohol dehydrogenase E chain	Cone	−46.4	78	1HN4	Phospholipase A2, major isoenzyme	Cone	−39.3

Table 1. continued

Rank	PDB	Protein name	Conformer	Affinity (kcal mol⁻¹)
29	1RLB	Retinol binding protein	Cone	-46.3
30	1W07	Peroxisomal acyl-coenzyme A oxidase 1	Cone	-46.2
31	1QD6	Phospholipase A1	Cone	-46.2
32	1CZ2	Non-specific lipid-transfer protein	Cone	-46.2
33	1K8Q	Gastric triacylglycerol lipase	Cone	-46.2
34	1AC4	Cytochrome c peroxidase, mitochondrial	Cone	-45.9
35	1EPB	Epididymal-specific lipocalin-5	Cone	-45.8
36	1RT6	HIV-1 reverse transcriptase	Cone	-45.7
37	1A7C	Plasminogen activator inhibitor 1	Cone	-45.7
38	1SPG	Carbonmonoxy hemoglobin	Cone	-45.2
39	1OI9	Cyclin-dependent kinase 2 (CDK2)	Cone	-45.1
40	2J0D	1,8-cineole 2-exo-monooxygenase	Cone	-44.5
41	4AAH	Methanol dehydrogenase [cytochrome c] subunit 1	Cone	-44.5
42	1ACM	Aspartate transcarbamoylase	Cone	-44.1
43	4DFR	Dihydrofolate reductase	Cone	-44.0
44	1HZX	Rhodopsin	Cone	-43.7
45	1COY	Cholesterol isomerase	Cone	-43.6
46	1R1K	Gene regulation protein	Cone	-43.5
47	1EFH	Sulfotransferase 2A1	Cone	-43.3
48	1ED5	Nitric oxide synthase	Cone	-43.2
49	1NEK	Succinate dehydrogenase flavoprotein subunit	Cone	-42.7
50	1TUB	Tubulin alpha-1A chain	1,2-Alternate	-42.3
79	1HDC	3-alpha-(or 20-beta)-hydroxysteroid dehydrogenase	Cone	-39.3
80	1SEZ	Protoporphyrinogen oxidase, mitochondrial	Cone	-39.2
81	1VFR	Major NAD(P)H-flavin oxidoreductase	Cone	-39.1
82	1POC	Phospholipase A2	Cone	-39.0
83	1R18	L-isoaspartyl protein carboxyl methyltransferase	Cone	-39.0
84	1GNX	Beta-glucosidase	Cone	-39.0
85	1GOS	Monoamine oxidase type B	Cone	-38.9
86	1DIS	Dihydrofolate reductase	Cone	-38.8
87	1HB2	Isopenicillin N synthase	Cone	-38.8
88	2UPJ	HIV-1 protease	Cone	-38.7
89	1CQZ	Cytosolic epoxide hydrolase 2	Cone	-38.6
90	1TFD	Serotransferrin	Cone	-38.4
91	3PGK	Phosphoglycerate kinase	Cone	-38.2
92	2SIM	Sialidase	1,2-Alternate	-38.2
93	1HJ1	Estrogen receptor beta	Cone	-38.2
94	2R07	Genome polyprotein	1,2-Alternate	-38.1
95	1UH5	Enoyl-ACP reductase	Cone	-38.1
96	1JP7	Purine nucleoside phosphorylase	Cone	-38.0
97	1PXX	Cyclooxygenase-2	1,2-Alternate	-37.9
98	2BO6	Mannosylglycerate synthase	Cone	-37.9
99	3HSC	ATPase fragment	Cone	-37.8
100	1OF7	Aldehyde dehydrogenase, mitochondrial	Cone	-37.6

Figure 2. A. Docked structure of calix[4]arene in the crystallographic structure of PPAR-α (1K7L).[58] **B.** Superposition of the crystallographic structure of stearic acid (in green, 6LX7)[57] and cipofibrate (in red, 6LX5)[57] and docked structure of calix[4]arene. **C.** $\Delta E_{binding}$ decomposed per residue. **D.** Graphical representation of the interaction between CysA276, SerA280 and IleA354 and calix[4]arene.

acid, as well as polyunsaturated fatty acids and other substances derived from fatty acids,[57] are examples of endogenous ligands. Fibrate drugs, which are used to treat hyperlipidemia, bind to PPAR-α.[57]

Calix[4]arene binds in the PPAR-α ligand binding domain (Figure 2A), representing an interesting lead compound for the development of innovative inhibitors of PPAR-α.

Calix[4]arene shares the same binding pocket of the most important endogenous PPARα ligand fatty acids ligands (Figure 2B), i.e. stearic and palmitic acids, that are the most common fatty acids that are released into the bloodstream during fasting. The best pose of calix[4]arene, identified "blindly" by the docking protocol, also superimposes with the crystal structure of ciprofibrate,[57] a well-known lipid-lowering agent. The fingerprint analysis of the calix[4]arene binding revealed that the most interacting amino acids are CysA276, SerA280 and IleA354, residues that were already identified as crucial components of the PPAR-α ligand binding domain (Figure 2C and D).[59] In particular, it is interesting the position of the CysA276, where the hydrophobic and "soft" sulfur fits perfectly within the aromatic cavity of the calixarene. This residue is conserved across all PPARs subtypes, and its crucial role for both the inhibitory effects and enhancing effects was already highlighted in previous studies.[59] The binding energy of calix[4]arene with PPAR-α ($\Delta E_{binding} = -61.9$ kcal mol^{-1}) was even higher than the binding energy of the protein with its natural substrate, i.e. the stearic acid ($\Delta E_{binding} = -57.7$ kcal mol^{-1}), or with agonists in clinical use such as ciprofibrate ($\Delta E_{binding} = -38.8$ kcal mol^{-1}), see Table S1.

Since the calix[4]arene binding site appears to be located deep between the alpha-helices of the protein, we calculated the accessible tunnels to reach this region (Figure S1A and B) and modeled the transport of the calix[4]arene from the solvent to the binding pocket (Figure S1C and D). The calculation clearly identified the accessibility of the binding site for the calix[4]arene and defined an exothermic pathway (Figure S1C and D) for the molecule from the outside of the protein to the binding site.

PPAR-α belongs to the subfamily of peroxisome proliferator-activated receptors, which also includes PPAR-δ and PPAR-γ. Interestingly, calix[4]arene binds also PPAR-γ (position 2 of the ranking) and PPAR-δ (position 10 of the ranking). These receptors are essential for controlling cellular development, differentiation, and metabolism (i.e. lipid, carbohydrate). They also play a crucial role in cancer pathogenesis and growth in higher species. Many commercial drugs bind PPAR-α and PPAR-γ, demonstrating the interest to identify new scaffolds for these molecular targets.

Nuclear receptors. Other nuclear receptors are also ranked highly. Nuclear receptors are a class of proteins responsible for sensing lipophilic substances such as hormones (i.e. steroids) or vitamins. These molecules usually bind and activate the nuclear receptors, regulating the expression of specific genes, which in turn control the organism's growth, homeostasis, and metabolism. Therefore, ligands that bind to these receptors can have a significant impact on the organism. About 13% of FDA-approved drugs in USA target nuclear receptors.[60]

Lipophilic compounds including vitamins A and D, fatty acids, retinoic acid, endogenous and xenobiotic hormones are

Chemistry–A European Journal

Research Article
doi.org/10.1002/chem.202400871

Chemistry Europe
European Chemical
Societies Publishing

examples of ligands that bind to and activate nuclear receptors. Calix[4]arene, due to its hydrophobicity and the chemical similarity to these ligands, is recognized by many nuclear receptors, binding in their ligand binding domains (Figure 3), with a binding energy generally higher than their natural substrate (Table S1).

In particular, among the first 100 positions, we identified estrogen receptors alpha (ERα) and beta (ERβ) (Erβ in position 5 and ERα in position 7, Figure 3A), the progesterone receptor (position 11, Figure 3B); the androgen receptor (position 12, Figure 3C), the androstane receptor (position 15, Figure 3D), the retinoic acid receptor RXR beta (RXRβ, position 18, Figure 3E), the nuclear receptor ROR beta (RORβ, position 23, Figure 3F),

the pregnane X Receptor (position 62, Figure 3G) and the retinoic acid receptor RXR alpha (RXRα, position 68, Figure 3H).

Special attention is here paid to the estrogen receptors due to their position in the top 10 proteins and their pharmacological relevance. Two subtypes of estrogen receptors can be identified: ERα and Erβ. Both ERα and Erβ are activated by the hormone estrogen (17β-estradiol). Hormone-activated estrogen receptors dimerize and since the two subtypes are co-expressed in various cell types, they can form homodimers such as ERα (αα) or ERβ (ββ) or heterodimers, such as ERαβ (αβ). ERα and Erβ exhibit a significant sequence homology. ER is a transcription factor that can translocate into the nucleus and bind to DNA. This translocation allows ER to control the activity of many genes.
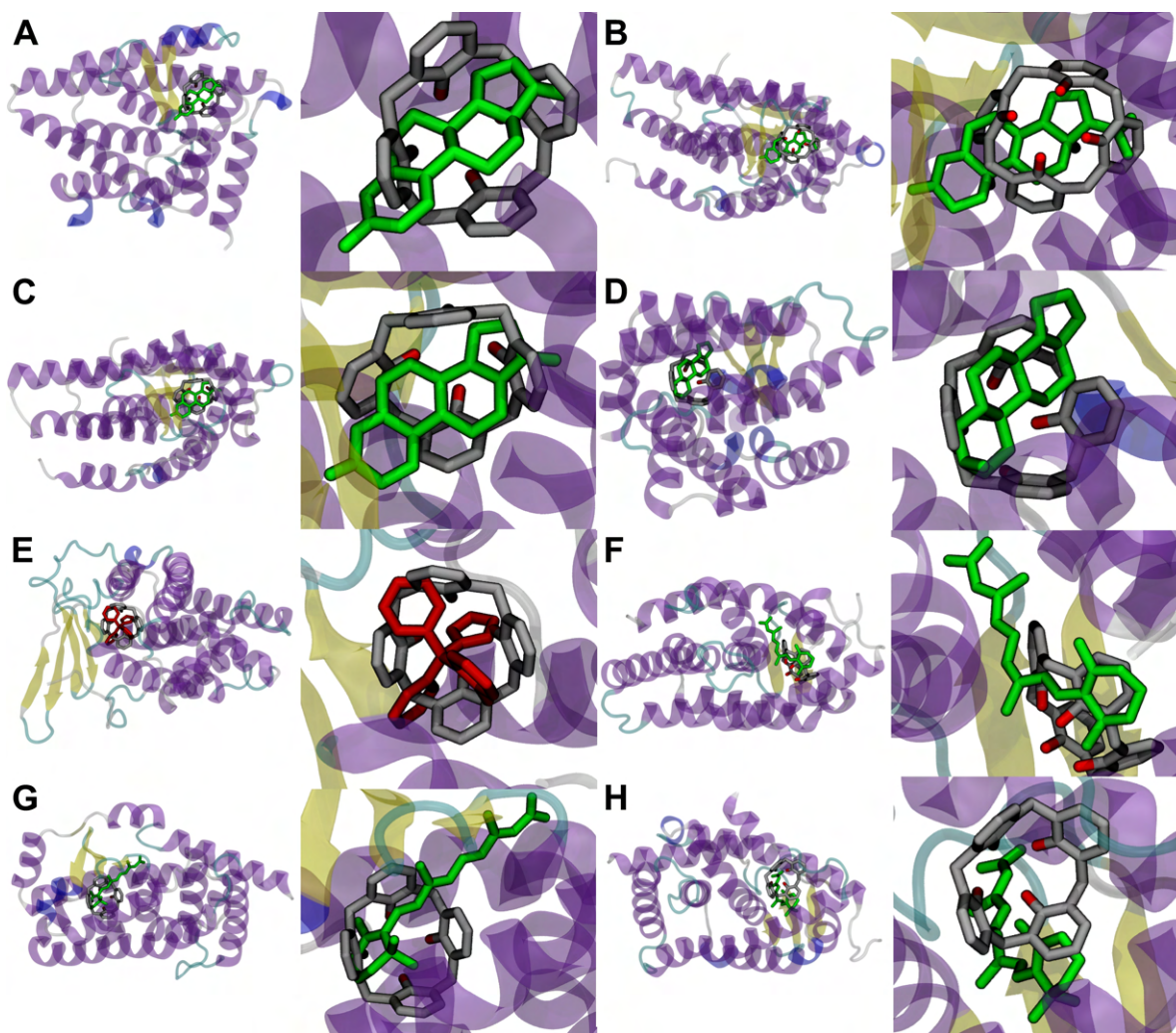
Figure 3. A. Superposition of the crystallographic structure of estradiol (in green, 2 J7X)[61] and docked structure of calix[4]arene in the crystallographic structure of the estrogen receptor beta (1QKM).[61] **B**. Superposition of the crystallographic structure of progesterone (in green, 1A28)[62] and docked structure of calix[4]arene in the crystallographic structure of progesterone receptor (1E3K).[63] **C**. Superposition of the crystallographic structure of testosterone (in green, 2AM9)[64] and docked structure of calix[4]arene in the crystallographic structure of androgen receptor (1E3G).[63] **D**. Superposition of the crystallographic structure of androstane (in green, 1XNX)[65] and docked structure of calix[4]arene in the crystallographic structure of androstane receptor (1XNX).[65] **E**. Superposition of the crystallographic structure of retinoic acid (in green, 4DM8)[66] and docked structure of calix[4]arene in the crystallographic structure of the retinoic acid receptor RXR beta (1UHL).[67] **F**. Superposition of the crystallographic structure of retinoic acid (in green, 1N4H)[68] and docked structure of calix[4]arene in the crystallographic structure of the nuclear receptor ROR-β (1K4W).[69] **G**. Superposition of the crystallographic structure of clotrimazole (in red, 7AXA)[70] and docked structure of calix[4]arene in the crystallographic structure of the pregnane X receptor (1ILH).[71] **H**. Superposition of the crystallographic structure of retinoic acid (in green, 3A9E)[72] and docked structure of calix[4]arene in the crystallographic structure of the retinoic acid receptor RXR-α (1DKF).[73]

Chem. Eur. J. **2024**, *30*, e202400871 (6 of 20)

© 2024 Wiley-VCH GmbH

RIGHTS LINK

Chemistry–A European Journal

Research Article
doi.org/10.1002/chem.202400871

Chemistry Europe
European Chemical
Societies Publishing

Overexpression of estrogen receptors is observed in about 70% of cases of breast cancer (ER+ breast cancers). ERs have also been implicated in ovarian, colon, prostate and endometrial cancer. Selective estrogen receptor modulators (SERMS), such as tamoxifen, act as ER antagonists in breast tissue and are used in endocrine therapy for breast cancer. In tumor cells and other tissue targets, tamoxifen binds to the ER in a competitive manner (in relation to the endogenous agonist estrogen), forming a nuclear complex that suppresses the effects of estrogen and reduces DNA synthesis.

Interestingly, calix[4]arene binds in the estrogen receptor–ligand-binding domain (Figure 4A) and perfectly superimposes with the natural ligand of ER, i.e. estradiol [74] and with competitive inhibitors, such as tamoxifen (Figure 4B).[75] This fact is perhaps not surprising considering the natural resemblance between calix[4]arene and the four fused rings of the steroids or the three conjugated aromatic rings of the tamoxifen molecule.

Calix[4]arene in ERα accommodates in the hydrophobic pocket formed by LeuA346, LeuA387, MetA388, PheA404, MetA421, and LeuA525. Analysis of the most interacting residues showed that calix[4]arene is sandwiched by the LeuA346 residue, that fits inside the cavity, and LeuA387/MetA388, that strongly interact with the external walls of the molecule.

pH-gated potassium channel KcsA. K+ channels are important targets in biomedical and pharmaceutical research,

because these membrane proteins are associated with a wide range of diseases, mostly nervous system disorders. Calixarene derivatives already demonstrated their ability to bind to the human voltage dependent potassium channel Kv1.2.[37] Modelling studies suggested that the conical platform of OH-free calixarenes were able to fully penetrate the extracellular outer vestibule of the Kv1.2 potassium channel.[37]

Here the docking results suggest that calix[4]arene can behave also as an intracellular ion channel blocker (Figure 5A) for the pH-gated potassium channel KcsA (position 6), in analogy to C_{60}, that fits into the channel pore and obstruct ion flow, impairing its functionality.[77]
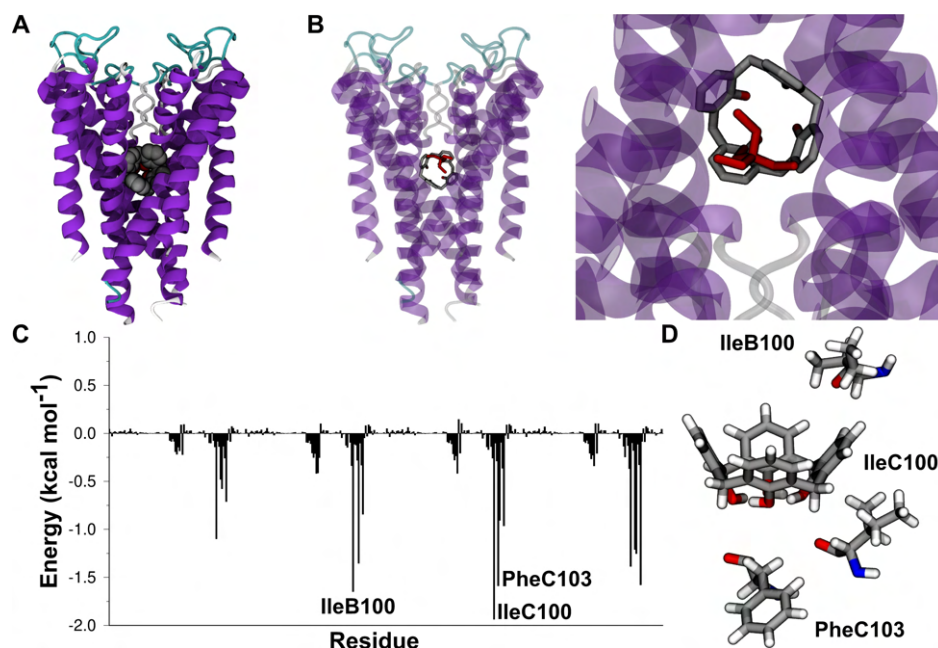
The position of the calix[4]arene coincides with the well-known inhibitor tetrabutylammonium (TBA) (Figure 5B), that inhibits almost all K+ channels, when acting intracellularly. [78] Since this site is highly conserved in different K+ channels, derivatives of calixarenes can be designed as efficient blockers of K+ channels.

Calix[4]arene binds in the inner cavity of KcsA that is lined mainly by hydrophobic amino acids (Ile100, Phe103). Fingerprint analysis (Figure 5C and 5D) showed that calix[4]arene strongly interacts via aromatic and hydrophobic interactions with these residues, in particular with Phe103 and two Ile100 (belonging to different subunits). Phe103 and Ile100 are also key residues in the functioning of the channel, in particular the rotameric state of Phe103 controls the conformational changes at the selectivity filter, leading to inactive states.[79]
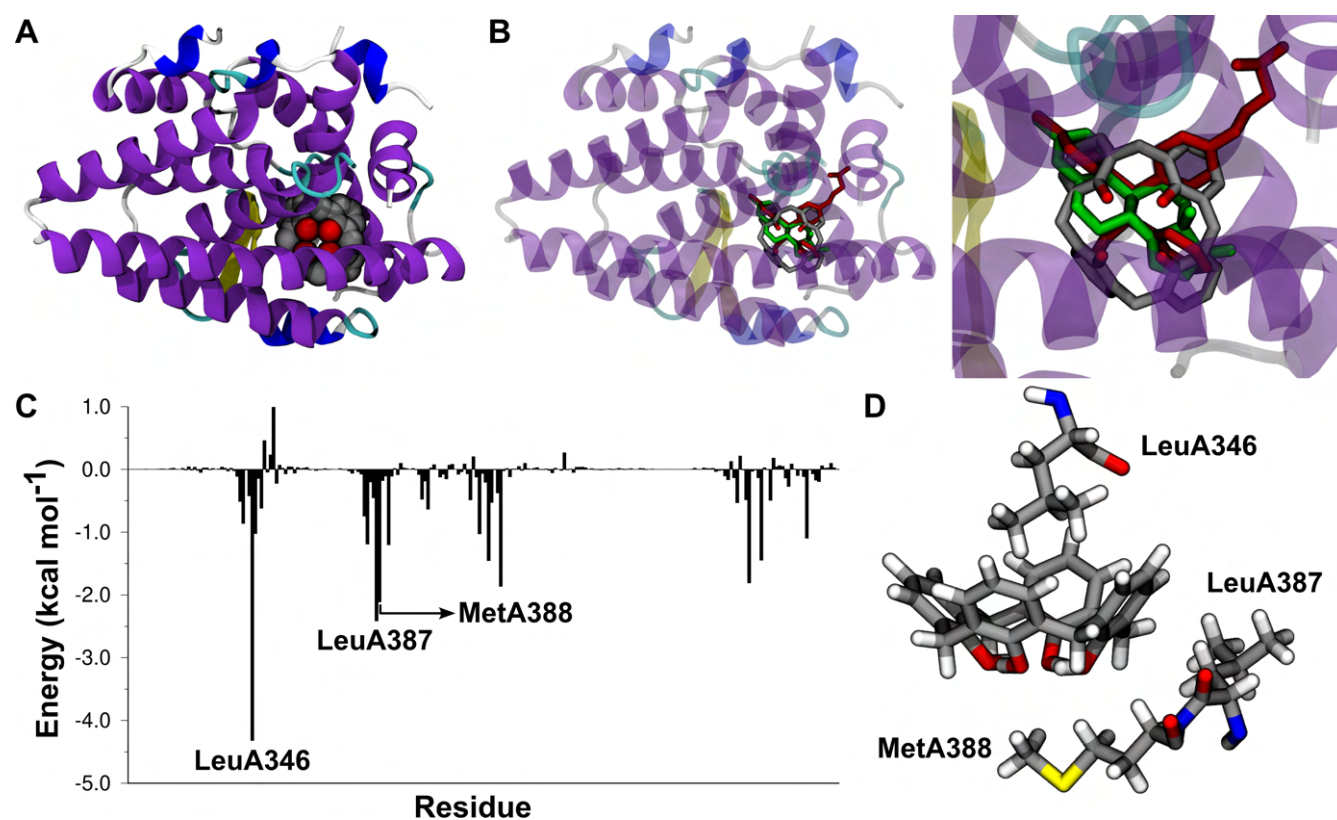
Figure 4. A. Docked structure of calix[4]arene in the crystallographic structure of estrogen receptor alpha (1PCG).[76] **B**. Superposition of the crystallographic structure of estradiol (in green, 5WGQ),[74] tamoxifen (in red, 5W9C)[75] and docked structure of calix[4]arene. **C**. $\Delta E_{binding}$ decomposed per residue. **D**. Graphical representation of the interaction between LeuA346, LeuA387 and MetA388 and calix[4]arene.

Chem. Eur. J. **2024**, 30, e202400871 (7 of 20)

© 2024 Wiley-VCH GmbH

Chemistry–A European Journal

Research Article
doi.org/10.1002/chem.202400871

**Chemistry
Europe**
European Chemical
Societies Publishing

Figure 5. A. Docked structure of calix[4]arene in the crystallographic structure of pH-gated potassium channel KcsA (1JVM).[78] **B**. Superposition of the crystallographic structure of tetrabutylammonium (in red, 1JVM)[78] and docked structure of calix[4]arene. **C**. $\Delta E_{binding}$ decomposed per residue. **D**. Graphical representation of the interaction between IleC100, IleB100 and PheC103 calix[4]arene.

Carrier proteins. Hydrophobic molecules, such fatty acids and hormones, are usually transported in the blood stream, or inside the cell, by specific proteins. Calix[4]arene can hijack these biomolecular systems and bind in place of the endogenous ligand (Figure 6) in oxysterol-binding protein (position 22), retinol binding protein (position 29), non-specific lipid-transfer protein (position 32); epididymal retinoic acid-binding protein (position 35) intestinal fatty acid-binding protein (position 58); bilin-binding protein (position 76).

Particularly interesting is the binding of calix[4]arene with plasma carrier proteins. Calix[4]arene derivatives can incorporate imaging agents for magnetic resonance imaging (MRI),[10] such as gadolinium ions.[16] The binding of a calix[4]arene-gadolinium complex to human serum albumin (HSA, position 59) or serotransferrin (position 90) can be exploited to develop innovative blood-pool agents for angiography.[16]

The binding of calix[4]arene with HSA deserves a special focus because this highly water-soluble is the most abundant protein in human blood. HSA is an endogenous carrier, responsible for the transport of hydrophobic molecules (i.e., bilirubin, thyroxine) in the blood. The transportation of fatty acids (FA) is one of the primary physiological functions of HSA. Seven fatty acid binding pockets (FA1-7) were crystallographically identified. HSA is also responsible for the transport in the blood of exogenous compounds, such as drugs. Drugs are usually bound at two primary sites: Sudlow site I or warfarin site (FA7) and Sudlow site II or ibuprofen site (FA3, FA4). Calix[4]arene binds to Sudlow site I (Figure 7A), in the hydrophobic cavity occupied by warfarin (Figure 7B).
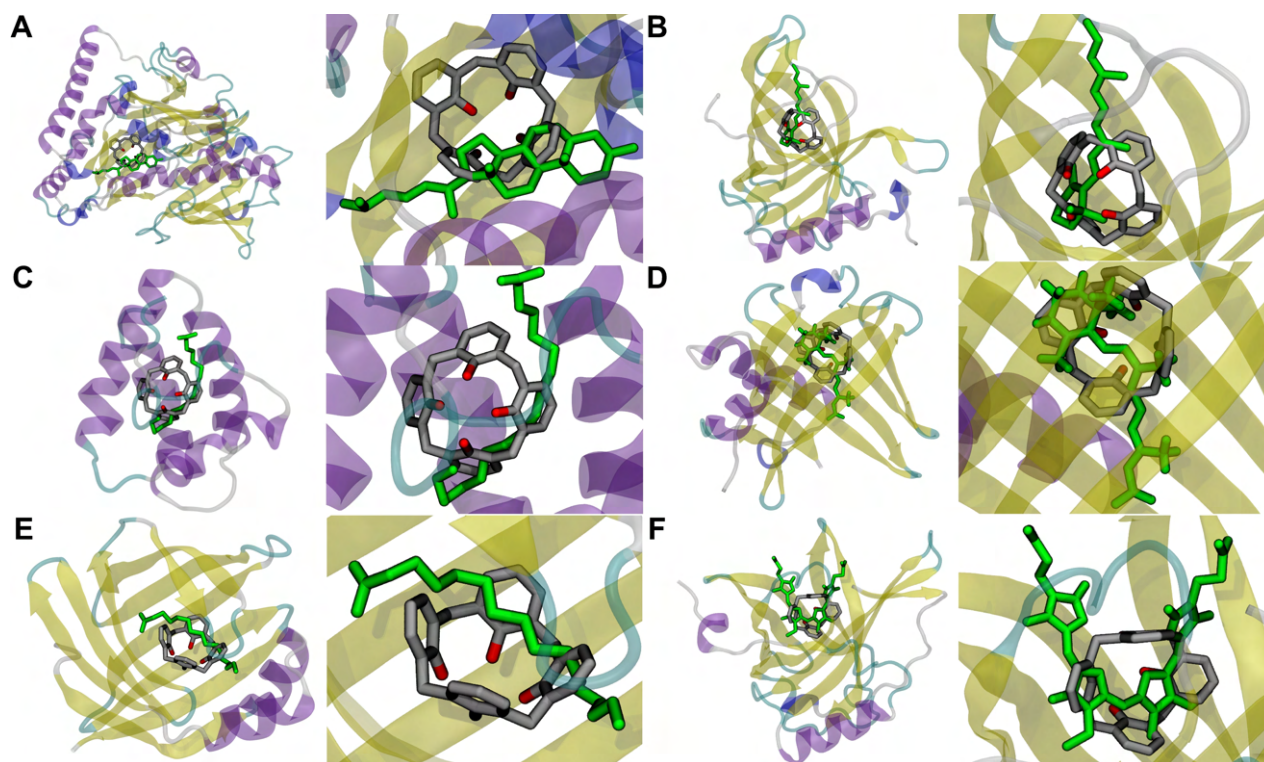
The roof and floor of the Sudlow site I are defined by the Ala291 and Leu238 residues. Many drugs bound at Sudlow site I are sandwiched between the side-chains of Leu238 and Ala291.

In this case, the methyl side chain of Ala291 is hosted by the calix[4]arene, strongly interacting with it (Figure 7C and D). Tyr150, that delimitates the warfarin binding pocket, also strongly interacts with calix[4]arene, in cooperation with His242 and Trp214, providing π-π interactions with the aromatic walls of the molecule. The interaction between calix[4]arene and Trp214 strongly resembles the one observed between the benzyl ring of warfarin and the side chain of Trp214, in that case a mutation of this residue reduces warfarin binding to HSA.[89] In contrast, in the case of His242, some differences can be observed comparing the binding of warfarin and calix[4]arene. ITC measurements demonstrated that the binding of warfarin induces protonation of His242. Such protonation establishes a stabilizing ion-pair interaction between the protonated His242 and the phenoxide group of warfarin.[90] In the docked structure, however, the interaction between calix[4]arene and His242 is purely π-π and therefore it should not influence its protonation states, as is also observed for the binding of other hydrophobic molecules in the Sudlow I site of HSA.[90]

In principle, all carrier proteins identified by the reverse docking approach can be used as a "Matryoshka system" to transport indirectly the ion/molecule trapped inside the calixarene host, strongly improving the limited solubility of the calixarenes in physiological environments.

Cancer-related proteins. The anticancer activity of calix[4]arene derivatives has already been highlighted.[8] The importance of the nuclear receptor proteins in cancer, discussed above, is well-known. Various cancer types have been linked to nuclear receptor malfunctioning and the targeting of this protein family represents a valid strategy for the development of cancer therapeutics, for example a significant increase in

Chem. Eur. J. **2024**, *30*, e202400871 (8 of 20)

© 2024 Wiley-VCH GmbH

Chemistry–A European Journal

Research Article
doi.org/10.1002/chem.202400871

Chemistry
Europe
European Chemical
Societies Publishing

Figure 6. A. Superposition of the crystallographic structure of cholesterol (in green, 7V62)[80] and docked structure of calix[4]arene in the crystallographic structure of the oxysterol-binding protein (1ZHY).[80] **B**. Superposition of the crystallographic structure of retinol (in green, 1RBP)[81] and docked structure of calix[4]arene in the crystallographic structure of the retinol binding protein (1RLB).[82] **C**. Superposition of the crystallographic structure of stearic acid (in green 1FK4)[83] and docked structure of calix[4]arene in the crystallographic structure of the non-specific lipid-transfer protein (1CZ2);[84] **D**. Superposition of the crystallographic structure of retinoic acid (in green, 1EPB)[85] and docked structure of calix[4]arene in the crystallographic structure of the epididymal retinoic acid-binding protein (1EPB);[85] **E**. Superposition of the crystallographic structure of palmitate (in green, 2IFB)[86] and docked structure of calix[4]arene in the crystallographic structure of the intestinal fatty acid-binding protein (2IFB);[86] **F**. Superposition of the crystallographic structure of biliverdin IX gamma (in green, 1BBP)[87] and docked structure of calix[4]arene in the crystallographic structure of the bilin-binding protein (1BBP).[87]
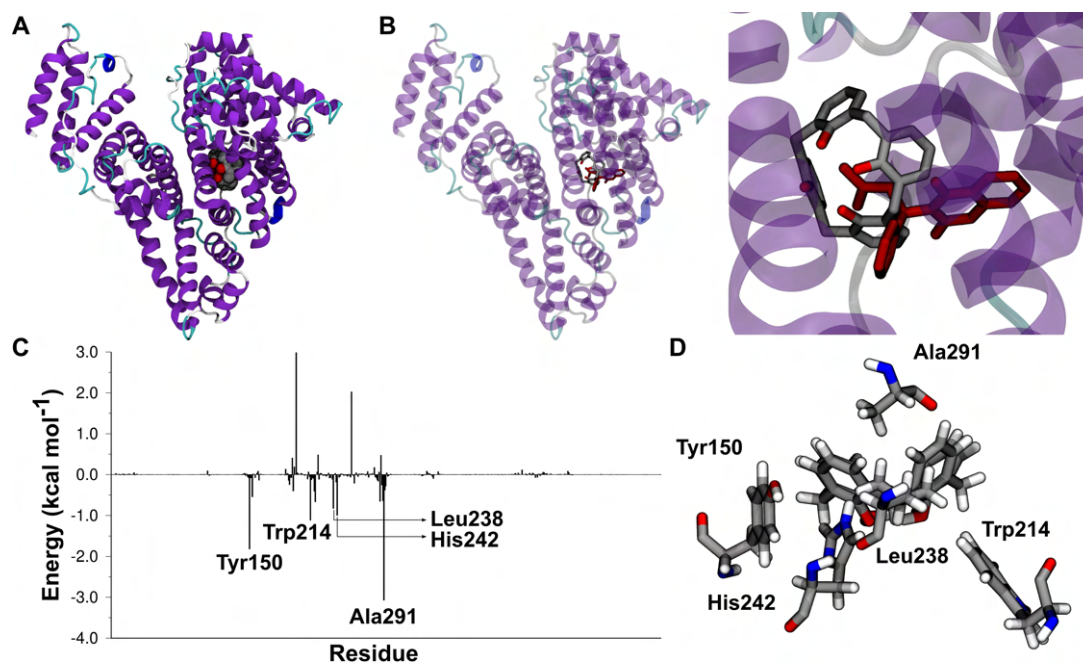
Figure 7. A. Docked structure of calix[4]arene in the crystallographic structure of human serum albumin (2BX8).[88] **B**. Superposition of the crystallographic structure of warfarin (in red, 2BXD)[88] and docked structure of calix[4]arene. **C**. $\Delta E_{binding}$ decomposed per residue. **D**. Graphical representation of the interaction between Ala291, Tyr150, Trp214, His242, Leu238 and calix[4]arene.

survival has been made possible by drugs that block the action of the androgen receptor (AR) in patients with prostate cancer or the ERα in patients with ERα+ breast cancer.

In the top 100 ranked proteins, the reverse docking approach identified other proteins that represent important therapeutic targets for cancer. For instance, i) protein kinases such as the cyclin-dependent kinase 2 (CDK2) in position 39 and the epidermal growth factor receptor (EGFR) tyrosine kinase in position 51, both involved in cell growth and signaling; ii) dihydrofolate reductase in position 53 that plays a key role in folate metabolism.

The inhibition of these targets may explain the anticancer activity of the calixarene derivatives and may offer the possibility to develop innovative inhibitors based on the calixarene scaffold. Inhibitor activity of CDK2 by calixarene derivatives were already suggested by Hamid et al.[91] considering the important structural similarities between calixarene derivatives and CDK2 inhibitors.[91]

CDK2 is crucial for controlling several aspects of the cell division cycle. The aberrant control of the cell cycle brought by CDK2 overexpression is an important factor in the hyper-proliferation of cancer cells. As a result, CDK2 is a possible therapeutic target for cancer treatment.

Calix[4]arene binds in the catalytic ATP-binding pocket of the CDK2 enzyme (Figure 8A), occupying the same region of the CDK2 inhibitor in clinical trial, roscovitine (Figure 8B).[93]

The binding of calix[4]arene is characterized by hydrophobic (IleA10, ValA18, ValA64, PheA80, Phe82 and LeuA134) interactions (Figure 8C and D) with those residues that physiologically form the binding pocket for the adenine base of the ATP.
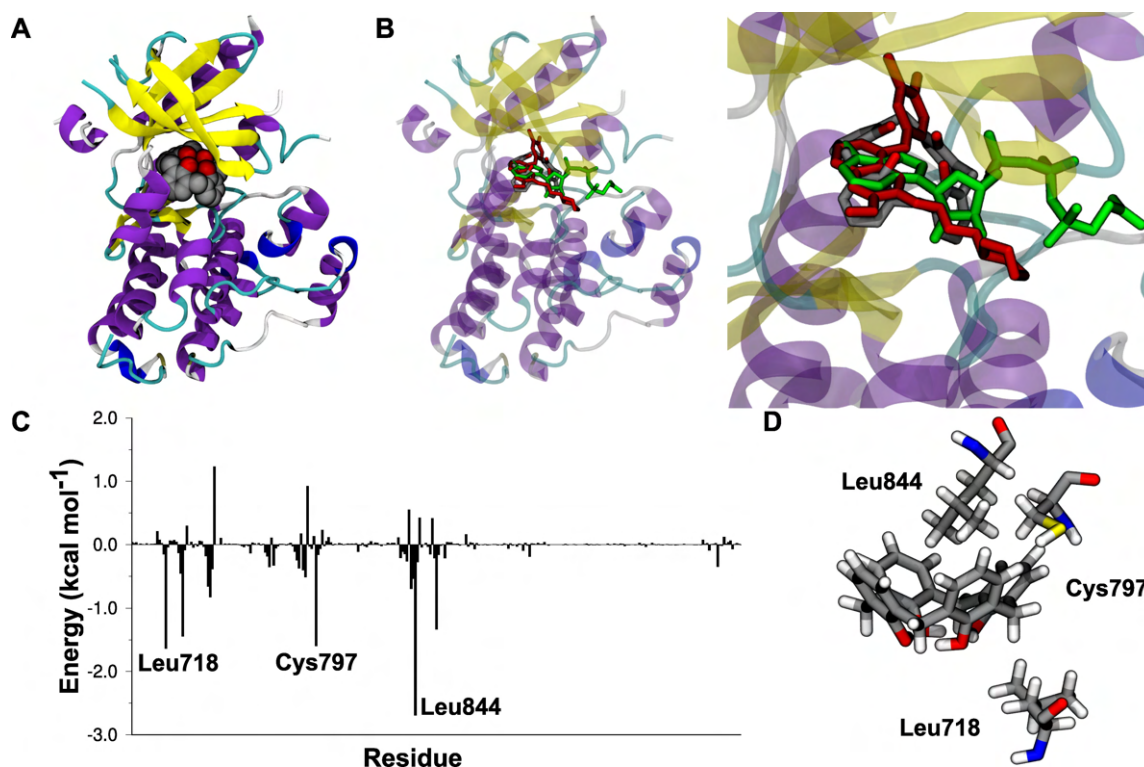
EGFR is a transmembrane tyrosine kinase receptor located at the cell surface. The binding of one of its natural ligands on the extracellular site induces cell proliferation and differentiation through the activation of the intracellular part of the receptor that contains a tyrosine kinase domain. EGFR activation is crucial in tumor growth and progression. Many cancer cells overexpress EGFR and for this reason, EGFR tyrosine kinase inhibitors (TKI) such as gefitinib, erlotinib, afatinib, brigatinib, icotinib and osimertinib, represent a very important class of drugs to fight cancer. In particular, targeted therapies against EGFR are promising treatments for different types of cancers.[94]

Calix[4]arene binds in the tyrosine kinase domain of EGFR, in the ATP-binding site of the enzyme (Figure 9A), in analogy with many TKI (Figure 9B). Comparing the binding mode of calix[4]arene with the crystallographic structure of gefitinib (Figure 9B), the first selective inhibitor of the EGFR tyrosine kinase domain, it is clear the overlap between the aromatic walls of the calix[4]arene and the aromatic rings of the drug. Residues Leu718, Val726, Ala743, Met793, and Leu844 form a core binding pocket for many inhibitors, that is highly hydrophobic and conserved.[97] These residues strongly interact also with the calix[4]arene (Figure 9C and D), sandwiched in particular by the two leucines (Leu844 and Leu718).
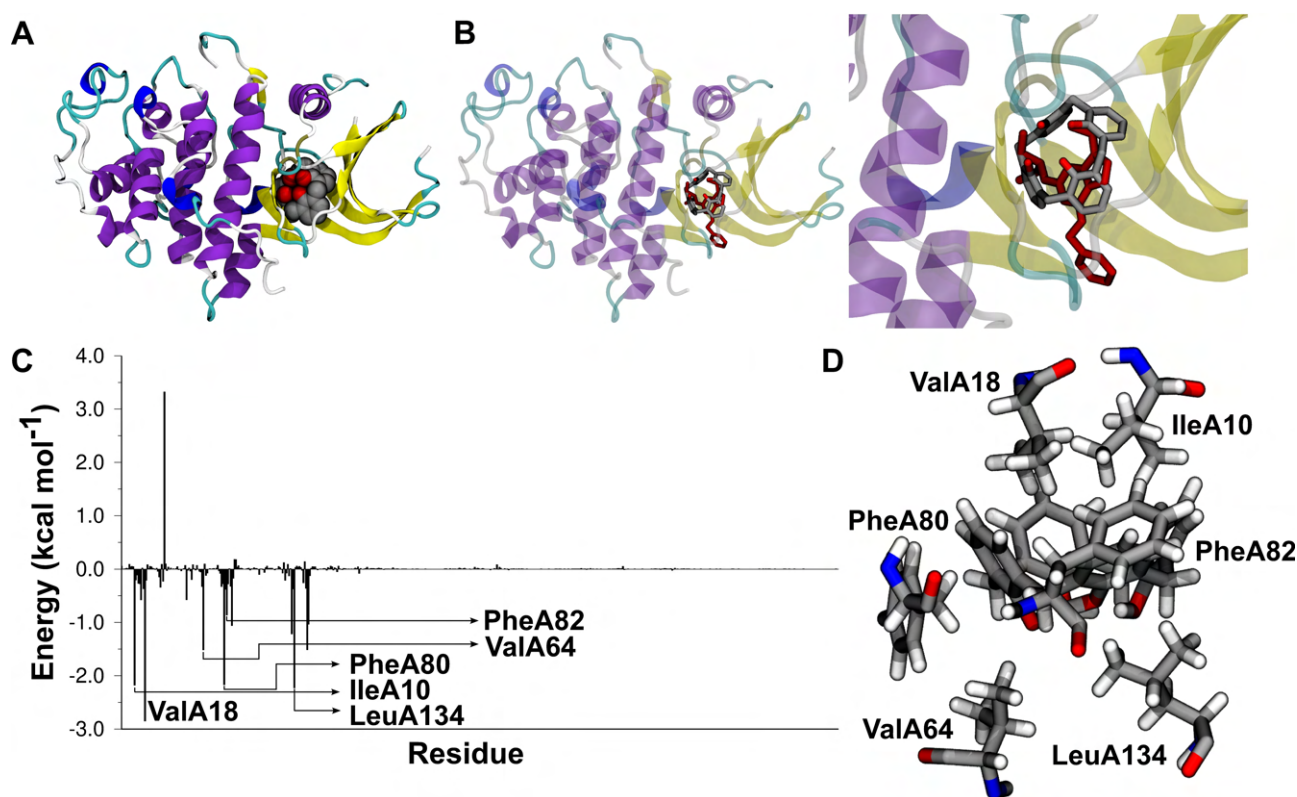
Figure 8. A. Docked structure of calix[4]arene in the crystallographic structure of cyclin-dependent kinase 2 (CDK2) (1OI9).[92] **B**. Superposition of the crystallographic structure of roscovitin (in red, 2A4L)[93] and docked structure of calix[4]arene. **C**. $\Delta E_{binding}$ decomposed per residue. **D**. Graphical representation of the interaction between IleA10, ValA18, ValA64, PheA80, Phe82 and LeuA134 and calix[4]arene.

Chemistry–A European Journal

Research Article
doi.org/10.1002/chem.202400871

Chemistry
Europe
European Chemical
Societies Publishing

Figure 9. A. Docked structure of calix[4]arene in the crystallographic structure of EGFR (1XKK).[95] **B**. Superposition of the crystallographic structure of gefniteb (in red, 4WKQ)[96] and ATP-analogue (in green, 2GS6) and docked structure of calix[4]arene. **C**. $\Delta E_{binding}$ decomposed per residue. **D**. Graphical representation of the interaction between CysA276, SerA280 and IleA354 and calix[4]arene.

Calix[4]arene interacts non-covalently also with Cys797, that is a conserved residue in the ATP-binding pocket, involved in the formation of irreversible EGFR inhibitors *via* Michael addition to form a covalent EGFR adduct. The C797S mutation of the covalent anchor site to a less reactive serine residue has emerged as a typical cause of acquired drug resistance for covalent EGFR inhibitors, while with calix[4]arene this mutation is ineffective due to the non-covalent nature of this interaction with Cys797.

Dihydrofolate reductase (DHFR) is another well-established therapeutic target in cancer treatment, raising substantial interest in the discovery of new compounds able to block its activity. Physiologically, DHFR reduces dihydrofolate to tetrahydrofolate, that is a cofactor essential for purine and thymidylate synthesis. Being involved in the biosynthesis of nucleic acid precursors, inhibition of DHFR slows down DNA synthesis and cell proliferation. Probably, the best-known clinical inhibitor of DHFR is methotrexate. Methotrexate has an affinity for DHFR that is roughly 1000 times greater than dihydrofolate.
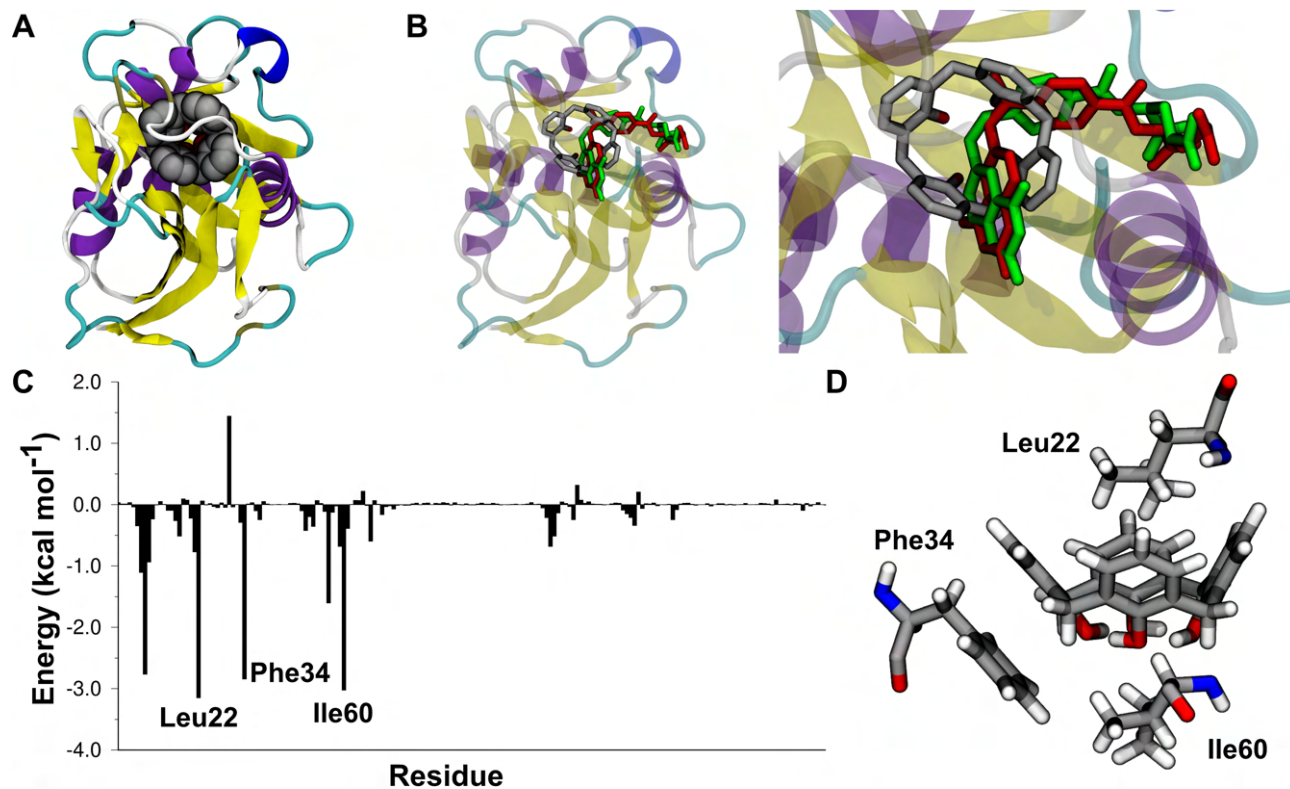
Calix[4]arene shares the same binding pocket of natural substrate of DHFR, i.e dihydrofolate (Figure 10A) and of its inhibitor, i.e. methotrexate (Figure 10B).[98] Again, the aromatic structure of the calix[4]arene occupies the protein binding pocket usually filled by the aromatic rings of the substrate/drug. Leu22 from the inside and Val8 and Phe34 from the outside squeeze the aromatic and hydrophobic structure of the calixarene (Figure 10C and D) *via* hydrophobic (Leu22 and Ile60) and π-π (Phe34) interactions.

Viral Proteins. It is widely known that calixarene derivatives have antiviral potential,[24,32,33] in particular, their ability to function as HIV inhibitors was demonstrated.[24,32,33]

Here the reverse docking procedure blindly recognizes HIV-1 reverse transcriptase (RT) as one of the most interacting protein with calix[4]arene (position 36). All retroviruses undergo a process known as retrotranscription, which transforms viral single strand RNA into a double strand DNA, that is then integrated into the host chromosome. This transcription is carried out by the enzyme RT. The human immunodeficiency virus, commonly recognized as the etiological agent of acquired immune deficiency syndrome (AIDS), encodes HIV-1 reverse transcriptase. Specific drugs were designed to impede the reverse transcriptase action, which HIV utilizes to replicate its genetic material and create new viruses (as part of a retrovirus proliferation cycle). Reverse-transcriptase inhibitors are a class of pharmaceuticals that includes nucleoside and nucleotide analogues or non-nucleoside inhibitors.

Calix[4]arene binds in the HIV-1 reverse transcriptase (Figure 11A) similarly to known inhibitors such as rilpivirine (Figure 11B),[101] a non-nucleoside reverse-transcriptase inhibitor.

Calix[4]arene overlaps with the three aromatic rings of rilpivirine and gives the usual host-guest interaction with LeuA100 and π-π interactions with TyrA181 and TyrA188 (Figure 11C and D). These two residues represent two of the most important amino acids belonging to the nonnucleoside RT inhibitor binding sites.

Chem. Eur. J. **2024**, *30*, e202400871 (11 of 20)

© 2024 Wiley-VCH GmbH

Chemistry–A European Journal

Research Article
doi.org/10.1002/chem.202400871

Chemistry Europe
European Chemical
Societies Publishing

Figure 10. **A**. Docked structure of calix[4]arene in the crystallographic structure of DHFR (1BOZ).[99] **B**. Superposition of the crystallographic structure of folate (in green, 1DHF)[100] and methotrexate (in red, 1RG7)[98] and docked structure of calix[4]arene. **C**. $\Delta E_{binding}$ decomposed per residue. **D**. Graphical representation of the interaction between Leu22, Ile60 and Phe34 and calix[4]arene.
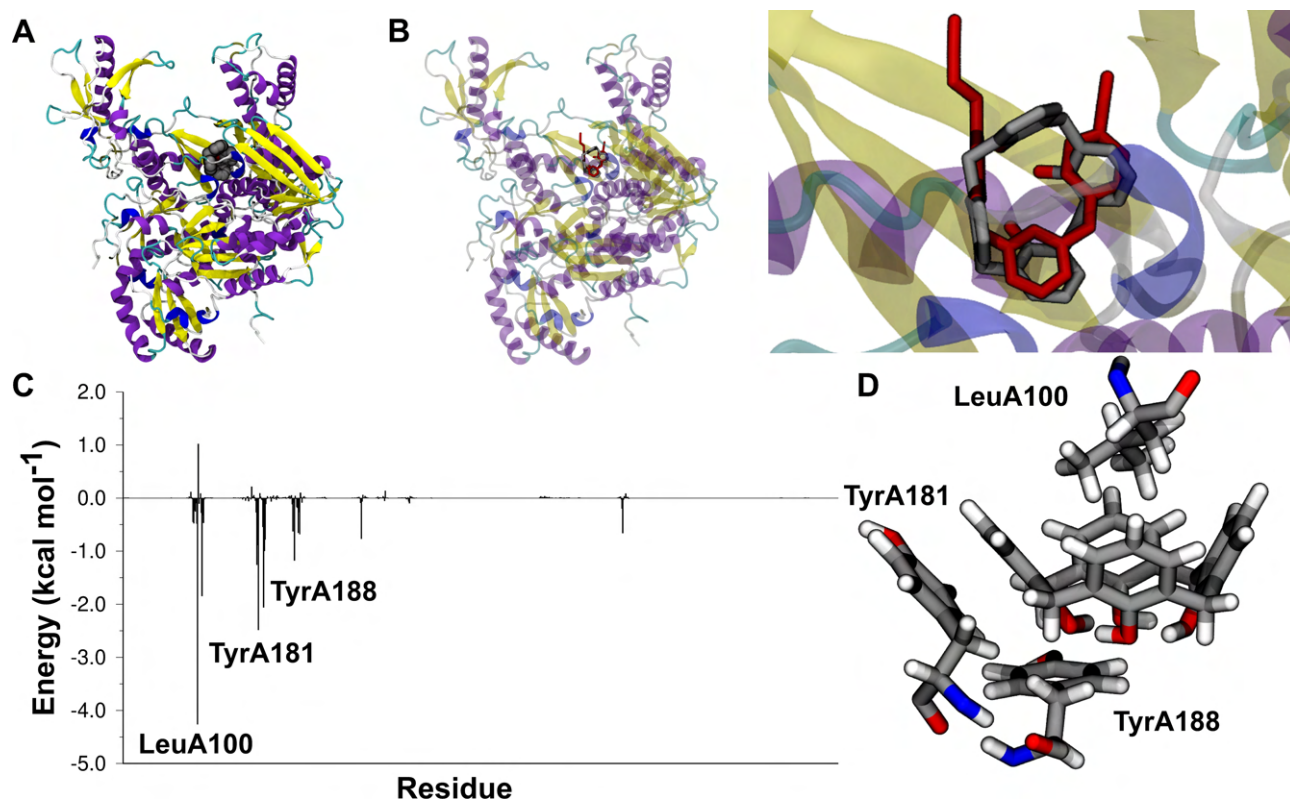
Figure 11. **A**. Docked structure of calix[4]arene in the crystallographic structure of HIV-1 reverse transcriptase (1RT6).[102] **B**. Superposition of the crystallographic structure of rilpivirine (in red, 6ELI)[101] and docked structure of calix[4]arene. **C**. $\Delta E_{binding}$ decomposed per residue. **D**. Graphical representation of the interaction between LeuA100, TyrA181 and TyrA188 and calix[4]arene.

Chemistry–A European Journal

Research Article
doi.org/10.1002/chem.202400871

Chemistry Europe
European Chemical
Societies Publishing

Interestingly, calix[4]arene binds also with HIV-protease (HIV-1 PR, position 57). The identification of this novel target could serve as the foundation for a novel multitargeted HIV therapy based on calix[4]arene derivatives. Calix[4]arene binds in the substrate binding region (Figure 12A), in analogy with clinical drugs such as amprenavir (Figure 12B).[103] HIV protease inhibitors are among the most important components in the combination therapy. HIV-1 PR breaks newly generated polyproteins at nine cleavage sites, generating the protein components of an HIV virion.

The active site of HIV-PR comprises residues Arg8, Leu23, Asp25, Gly27, Ala28, Asp29, Asp30, Val32, Lys45, Ile47, Met46, Gly48, Gly49, Ile50, Phe53, Leu76, Thr80, Pro81, Val82, Ile84.

Fingerprint analysis of the binding energy of calix[4]arene with HIV-PR (Figure 12C and D), reveals that calix[4]arene interacts diffusely with these active site residues, in particular, considering interaction energies higher that 1 kcal mol^{-1}, with AlaA28, ArgB8, LeuB23, ValB82, IleA47, IleA84, AspA25.

Calix[4]arene is also able to interact with the human rhinovirus capsid (position 94). Rhinoviruses (RV) are the main cause of the common cold. Amongst the best-known RV inhibitors there are drugs targeting the viral capsid. The capsid of the human rhinovirus is made up of 60 protomers arranged in an icosahedral symmetry (Figure 13A). Three surface viral proteins (VP1, VP2, and VP3) and a smaller internal protein (VP4) compose each protomer (Figure 13B and C). In the center of VP1 is present a hydrophobic pocket, usually occupied by a fatty acid-like molecule, or so-called 'pocket factor' that stabilizes the viral capsid. Many antiviral drugs bind to this hydrophobic pocket, taking the place of the pocket factor. This "irreversible" binding prevents the virus from uncoating and, in certain situations, blocks the attachment of viruses to host cell receptors, stopping the infection cycle and the spread of the virus.

In Figure 13D and E the superimposition of the calix[4]arene with pleconaril,[105] an effective drug against rhinovirus that binds to the hydrophobic pocket in VP1 major capsid protein. Calix[4]arene is sandwiched by Asn105 and Leu106 from one side and Tyr197, from the other side (Figure 13F and G). Calix[4]arene binds in the pore region, that gives access to the hydrophobic pocket, clogging the cavity and impeding the release of the pocket factor, exerting in this way an antiviral action.

The ideal calix[4]arene binding pocket. Considering the top-100 positions of the rank, we analyzed the per-residue decomposition analysis of the MM-GBSA interaction energy between the calix[4]arene and the proteins, to provide a statistical analysis of the most frequent amino acids involved during its binding. We considered all the residues with a binding energy higher than 2 kcal mol^{-1}. The frequency of these residues is compared to the natural abundance of the amino-acids (Figure 14).

From this analysis, it is clear the hydrophobic nature of the calix[4]arene and consequently that of the protein binding pockets host it. Hydrophobic aliphatic residues, characterized by branched-side chains, such as leucine (Leu, 23.5%), isoleucine (Ile, 11.3%) and valine (Val, 9.5%), are the most frequent binders. These hydrophobic residues can be in close contact both with the internal and external walls of the calix[4]arene.
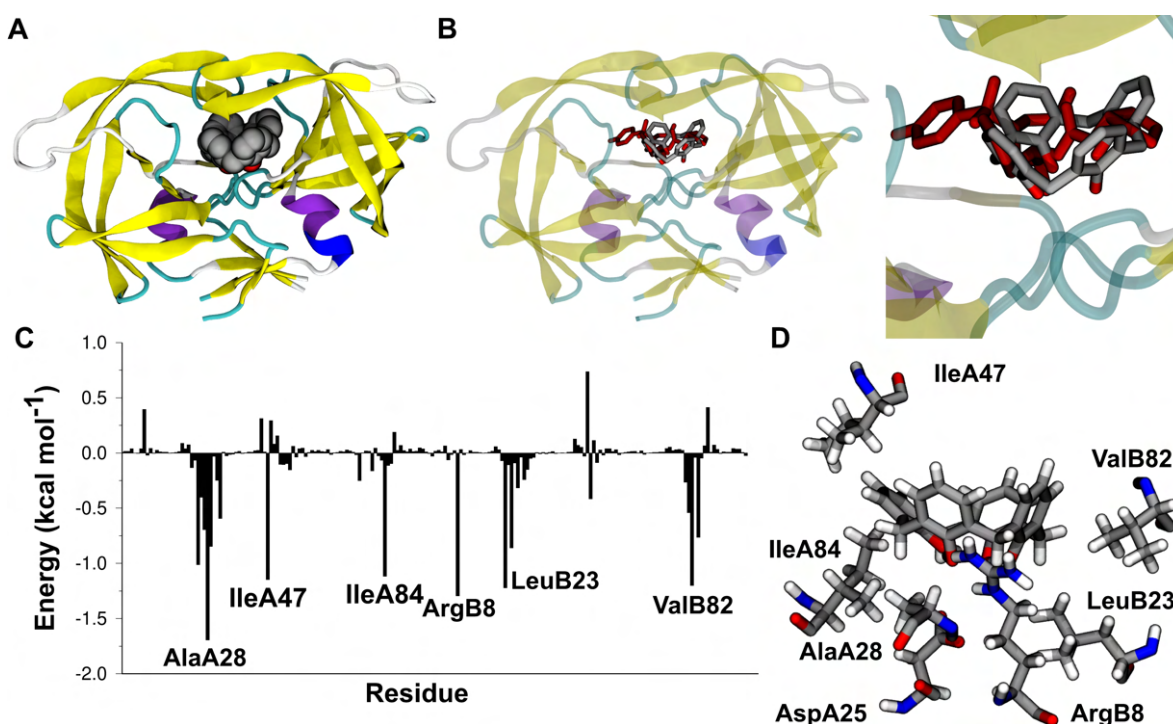
Figure 12. **A**. Docked structure of calix[4]arene in the crystallographic structure of HIV-1 protease (1HTE).[104] **B**. Superposition of the crystallographic structure of amprenavir (in red, 3NU3)[103] and docked structure of calix[4]arene. **C**. $\Delta E_{binding}$ decomposed per residue. **D**. Graphical representation of the interaction between AlaA28, IleA47, IleA84, ArgB8, ValB82 and LeuB23 and calix[4]arene.
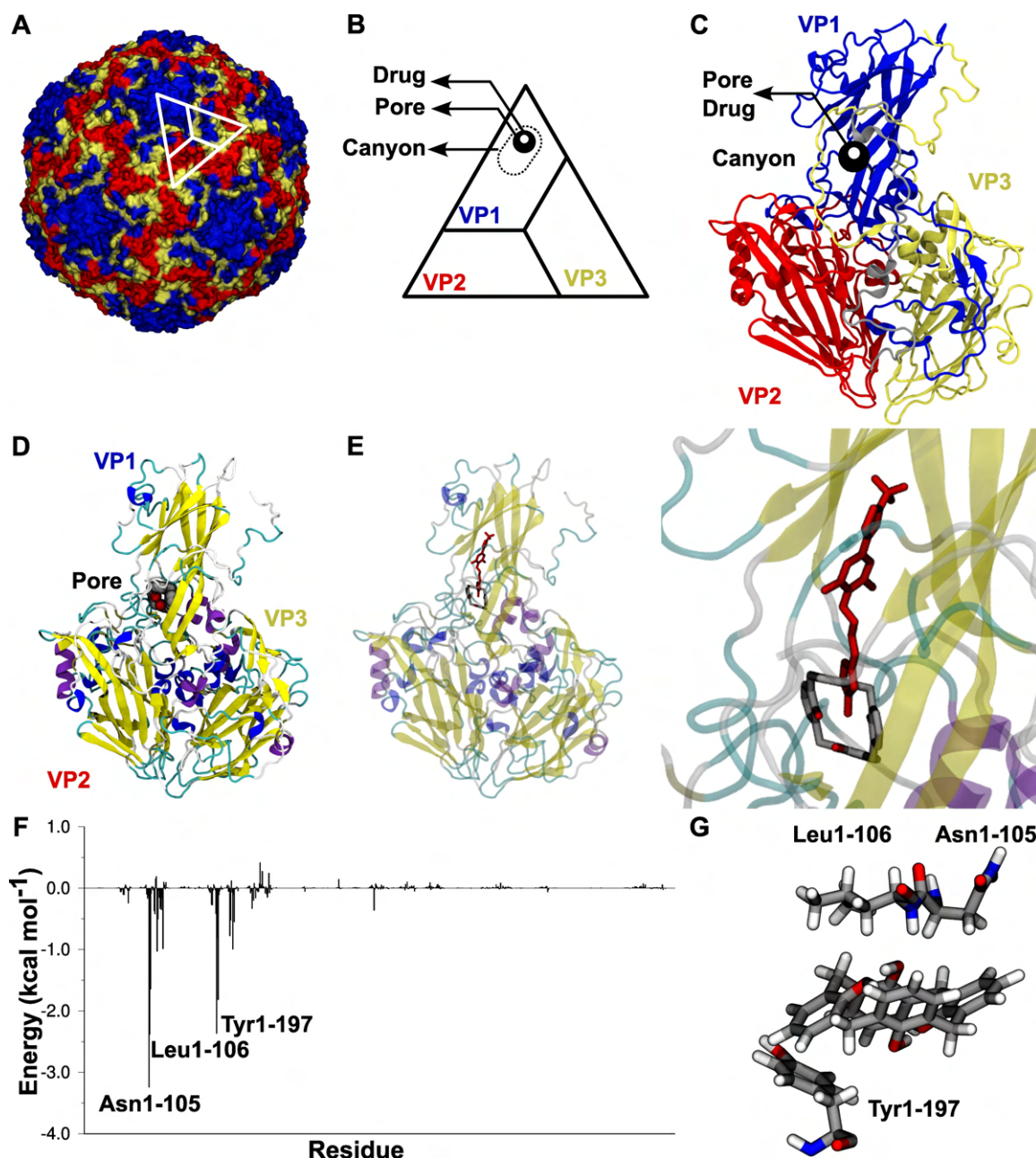
Figure 13. A. The RV–B14 capsid model with VP1 (blue), VP2 (red) and VP3 (yellow) proteins. **B**. Schematic representation of the VP1-3 trimer, the hydrophobic drug binding pocket extends from a pore at the base of the canyon into the VP1 central core. **C**. Cartoon representation of VP1-3 proteins with VP1 (blue), VP2 (red) and VP3 (yellow); the hydrophobic pocket is in VP1. **D**. Docked structure of calix[4]arene in the crystallographic structure of capsid of human rhinovirus (2R07).[106] **E**. Superposition of the crystallographic structure of pleconaril (in red, 1NCQ)[105] and docked structure of calix[4]arene. **F**. $\Delta E_{binding}$ decomposed per residue. **G**. Graphical representation of the interaction between Asn1-105, Leu1-106 and Tyr1-197 calix[4]arene.

Also, phenylalanines (Phe, 11.3%) frequently interact with the calix[4]arene, aligning their aromatic rings to the aromatic walls of the calixarene, optimizing in this way the π-π interactions, as reported in Figure 15.

When we compare the occurrence of "calix[4]arene binding residues" with their natural abundance, an enrichment is observed also for hydrophobic cysteines and methionines and aromatic histidines, tyrosines and tryptophanes (see Figure 14).

The analysis of the most-interacting amino acids (Table 2) identifies a strong tendency of the amino acid side chains to be embedded inside the cavity of the calixarene. Such most favored geometry of interaction recalls the classical host-guest assemblies (Figure 16A–C) that characterize the typical supramolecular interaction of calixarenes. Only for N–H hydrogen bond donor residues, such as asparagine, an interaction with the oxygen rims of the calixarene molecule is observed. We did not find any interactions of the oxygen rims with hydrogen bond acceptor amino acids, because the four hydroxyl groups are already occupied in intramolecular hydrogen bonds.
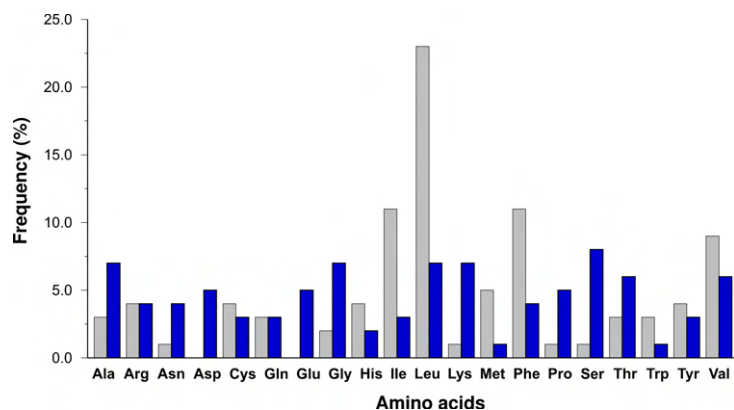
Chemistry–A European Journal

Research Article
doi.org/10.1002/chem.202400871

Chemistry Europe
European Chemical
Societies Publishing

Figure 14. Most frequent amino acids (%) responsible for the binding with calix[4]arene (grey bars) compared to their natural abundance (blue bars).
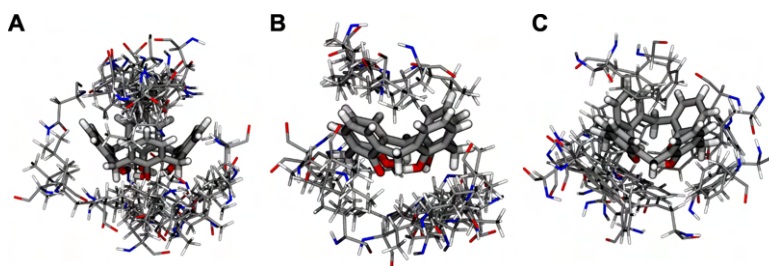

Figure 15. 3D-representation of the contacts between Leu (**A**), Ile (**B**) and Phe (**C**) with calix[4]arene.

Table 2. Highest interaction energies of the twenty proteinogenic amino acids with calix[4]arene in in the PDTD complexes. Energy contributions are reported in kcal mol^{-1}.

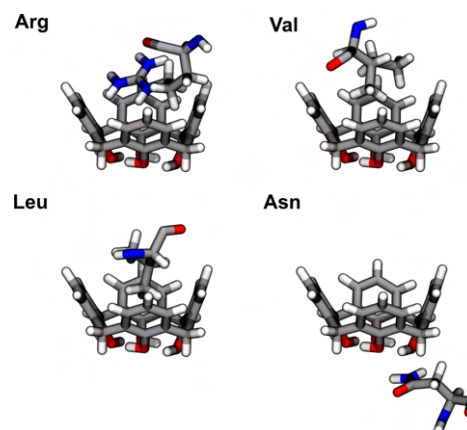| Residue	Energy contribution (kcal mol^{-1})	PDB
Arg288	−7.6	1FM6
Val246	−6.0	1BIF
LeuC40	−5.2	1QD6
Tyr423	−5.0	1W07
CysA276	−4.9	1K7L
Thr252	−4.9	1PHG
Ile339	−4.8	1UHL
TrpA237	−4.4	4AAH
Met406	−4.3	1DKF
Ser246	−3.9	1OF7
Phe56	−3.7	1IB1
ProA268	−3.4	1ACM
GlyA27	−3.3	2UPJ
LysA554	−3.1	1I19
Ala48	−3.0	1VE9
His89	−2.8	1SPG
GlnF117	−2.8	1RLB
Asn59	−2.4	1BBP
Glu746	−1.9	2A3L
Asp251	−1.1	1PHG

Figure 16. Most interacting geometries of Arg, Val, Leu and Asn with calix[4]arene in the PDTD complexes.

According to the decomposition of the binding energy in its components (Table 3), the van der Waals term (VDW) is the driving force of the binding.

Nonpolar solvation (ESURF), or hydrophobic interactions, facilitate the binding even though its value is much less than that of the vdW interactions. The electrostatic contribution (EEL) is small and significantly lower than the polar solvation term (EGB), that negatively affects the binding.

Hydrophilic amino acids, commonly present in protein binding pockets, upon formation of the complex with calix[4]arene, are forcedly desolvated, causing a destabilization of the system. Upon interaction with calix[4]arene these

RIGHTSLINK

Chemistry–A European Journal

Research Article
doi.org/10.1002/chem.202400871

Chemistry
Europe
European Chemical
Societies Publishing

Table 3. Energy components of $\Delta E_{binding}$.

PDB	TOTAL	VDW	EEL	EGB	ESURF
1K7L	−61.9	−58.2	−9.0	12.1	−6.8
1JVM	−53.5	−52.6	−6.6	12.3	−6.7
2BX8	−41.3	−51.8	−21.3	38.2	−6.4
1QKM	−55.0	−55.3	−1.8	9.4	−7.2
1PCG	−52.7	−52.2	−1.5	8.2	−7.2
1OI9	45.1	−53.1	3.6	11.0	−6.6
1XKK	−42.1	−47.7	−11.7	23.8	−6.5
1BOZ	−42.0	−55.0	−6.9	25.7	−5.8
1RT6	−45.7	−55.4	−4.8	21.3	−6.8
1HTE	−41.4	−51.6	−2.5	13.8	−6.1
2R07	−38.1	−52.0	−13.2	24.7	−6.6
1ZHY	−41.4	−50.6	−3.2	12.5	−6.6
1RLB	−46.3	−53.8	−8.6	22.8	−6.6
1CZ2	−46.2	−53.8	−1.6	15.8	−6.7
2IFB	−41.3	−50.0	−18.5	33.7	−6.5
1BBP	−39.4	−54.4	−6.5	28.1	−6.7
1UHL	−49.3	−49.6	−4.4	11.3	−6.3
1E3K	−50.5	−52.8	−5.5	14.2	−6.4
1E3G	−50.1	−52.9	−1.9	11.3	−6.6
1EPB	−45.8	−45.3	−5.1	11.3	−6.6
1P93	−49.5	−52.2	−5.6	14.7	−6.5
1K4W	−47.8	−49.5	−6.2	14.4	−6.5
1ILH	−40.7	−49.8	−3.8	18.8	−5.9
1DKF	−40.5	−48.4	−3.2	17.3	−6.1
1XNX	−49.5	−58.5	−0.7	15.9	−6.1

residues are screened with respect to the water molecules typically present in the binding pockets and can no longer interact with them because of the presence of the hydrophobic calix[4]arene molecule.

In general, the recognition and binding processes between proteins and calix[4]arene is governed by shape complementarity.

Ligand-based virtual screening. The reverse docking procedure that we used to identify potential calix[4]arene binding targets is a structure-based methodology. It could be interesting to integrate into this docking campaign an alternative procedure for virtual screening that employs different criteria. In particular, we identified a ligand-based methodology called SwissTarget.[107] SwissTarget predictions are performed by searching for molecules similar to calix[4]arene, in 2D and 3D, within a large collection of compounds known to be experimentally active on different macromolecular targets.[107] The top 15% of calix[4]arene protein targets, identified by the web-server SwissTarget, are illustrated in Figure S2 and Table S2, where "nuclear receptors" and "family A G-coupled receptors" emerge as the primary targets. Many nuclear receptors were already identified by the reverse docking procedure. In particular, estrogen receptor α tops the list (7th in our ranking), followed closely by estrogen receptor β (4th in the ligand-based

virtual screening and 5th in reverse docking). For the estrogen receptor α, we provided the molecules, identified by SwissTarget using the 2D (Figure S3) and 3D (Figure S4), with criteria of similarity for calix[4]arene.

Both methodologies identify also androgen receptors as significant targets for calixarene (12th in the reverse docking and 17th in ligand-based virtual screening) and nuclear receptors ROR (15th in ligand-based virtual screening and 23th in the reverse docking).

Many other proteins (cyclooxygenases, serine/threonine-protein kinase, cyclin dependent kinases, K^+ channels, monoamine oxidase, tyrosine protein kinase) were identified by both procedures, vouching for the reliability of the predictions.

Conclusions

In conclusion, here we developed a rational approach, based on reverse docking calculations, to identify potential drug targets of calix[4]arene, using it as a bait to fish out specific proteins from a database of druggable proteins (PDTD).

Despite the inherent limitations of the docking procedures, the virtual screening approach is able to select the most promising proteins able to specifically bind calix[4]arene, providing a prioritized list to rationally guide the study of calix[4]arene-protein complexes.

We identified many proteins of pharmaceutical interest such as:
(1) nuclear receptors (peroxisome proliferator-activated receptors, estrogen receptors, progesterone receptor, androgen receptor, androstane receptor, glucocorticoid receptor, retinoic acid receptor, nuclear receptor ROR-β and pregnane X receptor);
(2) potassium channels;
(3) cancer-related proteins (cyclin-dependent kinase 2, epidermal growth factor receptor tyrosine kinase and dihydrofolate reductase);
(4) viral proteins (HIV reverse transcriptase, HIV protease and human rhinovirus capsid).

Superpositions of the docked structures of calix[4]arene with the crystallographic structures of the proteins that are complexed with known drugs showed that the aromatic system of the calix[4]arene usually overlaps with the aromatic rings of the drug. Since calixarenes may be structurally modified and functionalized in a variety of ways, calix[4]arene may represent an excellent molecular scaffold for creating targeted enzyme inhibitors.

Considering the chemical similarity of calix[4]arene with many endogenous molecules such as hormones, it will be also possible to hijack the transport system of this molecules to carry calix[4]arene in the human body. The docking procedure showed that in many carrier proteins (oxysterol-binding protein, retinol binding protein, non-specific lipid-transfer protein, epididymal retinoic acid-binding protein, intestinal fatty acid-binding protein; bilin-binding protein, human serum albumin, serotransferrin) calix[4]arene can bind in place of the endogenous ligand. In principle, all these carrier proteins can be used

in a "Matryoshka-like system" to transport indirectly the ion/molecule trapped inside the calixarene, developing innovative theranostic platforms.

In many cases, the binding energy of calix[4]arene with these proteins is higher than that with the natural substrates of the proteins or with drugs in clinical use (Table S1).

A complementary ligand-based methodology confirmed the nuclear receptors, and in particular hormone-binding receptors, as primary targets for the calix[4]arene binding.

The statistical analysis of all the complexes between calix[4]arene and proteins showed that leucine, isoleucine, phenylalanines and valine are the most frequent binding residues, followed by hydrophobic cysteines and methionines and aromatic histidines, tyrosines and tryptophanes. In general, the recognition and binding processes between proteins and calix[4]arene is governed by shape complementarity, where the van der Waals term is dominating. Calix[4]arene appears mostly sandwiched by amino acid residues interacting at the same time with the inner part of its cavity and with the external walls.

Computational Methods

Quantum Mechanics Calculations

Conformational analysis. The relative energies of the four conformers of calix[4]arene (cone, partial cone, 1,2-alternate, 1,3-alternate) were determined using Density Functional Theory (DFT) with the m06-2x[108] functional and the 6–311++G** basis set.[109] To account for solvation effects, the Integral Equation Formalism Polarizable Continuum Model (IEFPCM) approach was employed.[110] All quantum mechanics calculations were performed using the Gaussian16 suite of programs.[109]

Calixarene parametrization. Calix[4]arene was parametrized using the GAFF force field.[111] Atomic charges for the calix[4]arene conformers were determined using the Merz-Singh-Kollman scheme[112] at the HF/6-31G* level.

Virtual Screening

Potential Drug Target Database (PDTD). The Potential Drug Target Database (PDTD) contains 1207 entries covering 841 known and potential drug targets with structures obtained from the Protein Data Bank (PDB).[113] To consider protein flexibility, PDTD includes redundant entries for proteins known to be flexible, allowing ensemble docking calculations.

Docking calculations. All the four conformers of the calix[4]arene were considered in the docking studies. Global docking (or blind docking) procedures that searches for all the possible binding sites of the ligand on the entire protein surface were used. Two different protein rankings were obtained using the PatchDock[114] and FireDock[115] algorithms. The scoring function used by these algorithms describe accurately the binding of proteins with rigid and hydrophobic moieties, such as photosensitizers,[116–118] fullerenes,[119–123] carboranes[124,125] and carbon nanotubes.[126,127]

PatchDock[114] is a rigid/soft docking algorithm. With a ligand and a protein structure as input, PatchDock uses a fast Fourier transform (FFT) algorithm to allow an efficient global docking search, maximizing the shape complementarity and minimizing steric repulsions. PatchDock initially divides the surfaces of the protein

and the ligand into patches based on the surface morphology (concave, convex, or flat). Next, it creates a list of potential transformations by using the geometric hashing algorithm to match flat patches with flat patches and concave patches with convex patches. A scoring function that estimates the shape complementarity and the atomic desolvation energy[128] of the complex is used to assess each pose. Since the approach permits some penetrations between the ligand and the protein, it implicitly takes into account, at least partly, protein/ligand flexibility and dynamics.

FireDock[115] takes as initial input PatchDock poses, but is a flexible docking methodology, that generates the geometry of interactions following an optimization step that adjusts the conformations of the amino-acid side-chains (rotamers) around the ligand. Following the rearrangement of the side-chains, the relative position of the docking partners are further refined by a Monte Carlo minimization.[129] All the obtained poses are then ranked by a scoring function that considers the van der Waals and electrostatic interactions, explicit hydrogen and disulfide bonds contributions, π-π-stacking, cation-π and aliphatic interactions. The force field parameters used in the scoring function derive from CHARMM19. The desolvation free energy of the binding process is estimated using, as solvation model, the effective atomic contact energies (ACE).[128]

Docking rescoring. Using a hierarchical approach, the top 500 complexes of the PatchDock and FireDock rankings were rescored (Scheme 1).

A molecular mechanics minimization of the complex was carried out. The Amber FF14SB force field was utilized to model the proteins.[130] Docked complexes underwent geometry optimization using SANDER:[131] 500 steepest descend minimization steps followed by an additional 500 conjugate gradient steps were
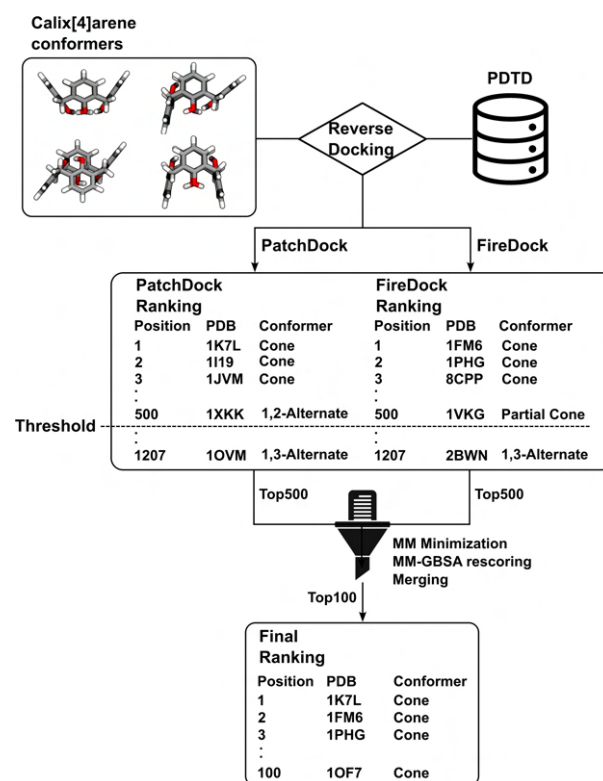
Scheme 1. Schematic representation of the hierarchical virtual screening procedure used in this article.

Chemistry–A European Journal

Research Article
doi.org/10.1002/chem.202400871

Chemistry Europe
European Chemical
Societies Publishing

carried out in Generalized Born (GB) implicit solvent model.[132] The optimized structures were used as input for MM-GBSA calculations,[133] to obtain the binding affinity of the different protein-calix[4]arene systems.[132] This procedure was recently validated to calculate the binding energy of calixarene derivatives to proteins.[134–136] Electrostatic and van der Waals (vdW) interactions were calculated considering an infinite cut-off. The polar solvation term was calculated using the GB model, whereas the non-polar solvation term was determined using solvent-accessible, surface-area-dependent terms. An energy penalty was applied to the binding energy when it binds in a different conformation from the most stable (cone conformation). A final ranking was obtained merging the results obtained by PatchDock and FireDock, both rescored at the MM-GBSA level (Table 1). The ability of this docking protocol was validated by a "bound docking" procedure, using two crystallographic structures (PDB IDs: 8R3B and 8R3C) of a calixarene derivative bound inside the concave pocket of a protein.[137]

Identification of ligand-binding pathways. We used the program CAVER[138] to calculate the protein tunnels and identify the accessible paths for the calix[4]arene to reach its binding sites. To model the transport of the calix[4]arene from the outside environment into the protein binding sites, we used the program CaverDock,[139] determining the trajectory of the ligand and the energy profile of the process.

Ligand-based virtual screening. For the ligand-based virtual screening we used the SwissTarget web-server,[107] that allows the estimation of the most probable macromolecular targets of a small molecule. The prediction based on a combination of 2D and 3D similarity with a library of 370000 known active molecules. Here we searched similarities only with compounds active on human proteins (2092 proteins).

Acknowledgements

Conflict of Interests

The authors declare no conflict of interest.

Data Availability Statement

The data that support the findings of this study are available from the corresponding author upon reasonable request.

[1] Y. C. Pan, X. Y. Hu, D. S. Guo, *Angew. Chem. - Int. Ed.* **2021**, *60*, 2768–2794.
[2] S. B. Nimse, T. Kim, *Chem. Soc. Rev.* **2013**, *42*, 366–386.
[3] E. Da Silva, A. Lazar, A. Coleman, *J. Drug Delivery Sci. Tech* **2004**, *14*, 3–20.
[4] M. Giuliani, I. Morbioli, F. Sansone, A. Casnati, *Chem. Commun.* **2015**, *51*, 14140–14159.
[5] V. Bohmer, *Angew. Chem. - Int. Ed.* **1995**, *34*, 713–745.
[6] L. Baldini, A. Casnati, F. Sansone, *Eur. J. Org. Chem.* **2020**, *2020*, 5056–5069.
[7] B. Mokhtari, K. Pourabdollah, *J. Inclusion Phenom. Macrocyclic Chem.* **2012**, *73*, 1–15.
[8] A. Yousaf, S. A. Hamid, N. M. Bunnori, A. A. Ishola, *Drug Des. Dev. Ther.* **2015**, *9*, 2831–2838.
[9] S. Paul, R. S. Jeyaprakash, A. Pai, H. Venkatachalam, B. S. Jayashree, *Med. Chem.* **2023**, *19*, 939–945.
[10] E. M. Georgiev, D. M. Roundhill, *Inorg. Chim. Acta* **1997**, *258*, 93–96.
[11] D. T. Schühle, J. A. Peters, J. Schatz, *Coord. Chem. Rev.* **2011**, *255*, 2727–2745.
[12] Y. Y. Wang, Y. Kong, Z. Zheng, W. C. Geng, Z. Y. Zhao, H. Sun, D. S. Guo, *Beilstein J. Org, Chem.* **2019**, *15*, 1394–1406.
[13] R. Kumar, A. Sharma, H. Singh, P. Suating, H. S. Kim, K. Sunwoo, I. Shim, B. C. Gibb, J. S. Kim, *Chem. Rev.* **2019**, *119*, 9657–9721.
[14] M. Massi, M. I. Ogden, *Materials* **2017**, *10*, 1369.
[15] T. Läppchen, R. P. M. Dings, R. Rossin, J. F. Simon, T. J. Visser, M. Bakker, P. Walhe, T. Van Mourik, K. Donato, J. R. Van Beijnum, A. W. Griffioen, J. Lub, M. S. Robillard, K. H. Mayo, H. Grüll, *Eur. J. Med. Chem.* **2015**, *89*, 279–295.
[16] S. Aime, A. Barge, M. Botta, A. Casnati, M. Fragai, C. Luchinat, R. Ungaro, *Angew. Chem. - Int. Ed.* **2001**, *40*, 4737–4739.
[17] R. Zadmard, N. S. Alavijeh, *RSC Adv.* **2014**, *40*, 41529–41542.
[18] P. B. Crowley, *Acc. Chem. Res.* **2022**, *55*, 2019–2032.
[19] M. L. Rennie, G. C. Fox, J. Pérez, P. B. Crowley, *Angew. Chem. - Int. Ed.* **2018**, *130*, 13960–13965.
[20] R. Kamada, W. Yoshino, T. Nomura, Y. Chuman, T. Imagawa, T. Suzuki, K. Sakaguchi, *Bioorg. Med. Chem. Lett.* **2010**, *20*, 4412–4415.
[21] M. A. Blaskovich, Q. Lin, F. L. Delarue, J. Sun, H. S. Park, D. Coppola, A. D. Hamilton, S. M. Sebti, *Nat. Biotechnol.* **2000**, *18*, 1065–1070.
[22] H. Zhou, D. A. Wang, L. Baldini, E. Ennis, R. Jain, A. Carie, S. M. Sebti, A. D. Hamilton, *Org. Biomol. Chem.* **2006**, *4*, 2376–2386.
[23] E. V. Lugovskoy, P. G. Gritsenko, T. A. Koshel, I. O. Koliesnik, S. O. Cherenok, O. I. Kalchenko, V. I. Kalchenko, S. V. Komisarenko, *FEBS J.* **2011**, *278*, 1244–1251.
[24] L. K. Tsou, C. H. Chen, G. E. Dutschman, Y. C. Cheng, A. D. Hamilton, *Bioorg. Med. Chem. Lett.* **2012**, *22*, 3358–3361.
[25] F. Sansone, L. Baldini, A. Casnati, R. Ungaro, *New J. Chem.* **2010**, *34*, 2715–2728.
[26] R. P. M. Dings, X. Chen, D. M. E. I. Hellebrekers, L. I. van Eijk, Y. Zhang, T. R. Hoye, A. W. Griffioen, K. H. Mayo, *J. Natl. Cancer Inst.* **2006**, *98*, 932–936.
[27] I. Morbioli, V. Porkolab, A. Magini, A. Casnati, F. Fieschi, F. Sansone, *Carbohydr. Res.* **2017**, *453–454*,, 36–43.
[28] M. Ali, K. D. Daze, D. E. Strongin, S. B. Rothbart, H. Rincon-Arano, H. F. Allen, J. Li, B. D. Strahl, F. Hof, T. G. Kutateladze, *J. Biol. Chem.* **2015**, *290*, 22919–22930.
[29] Z. Wang, S. Tao, X. Dong, Y. Sun, *Chem. Asian J.* **2017**, *12*, 341–346.
[30] M. Mallon, S. Dutt, T. Schrader, P. B. Crowley, *ChemBioChem* **2016**, *17*, 774–783.
[31] S. Gordo, V. Martos, E. Santos, M. Mené Ndez, C. Bo, E. Giralt, J. De Mendoza, *PNAS* **2008**, *105*, 16426–16431.
[32] L. K. Tsou, G. E. Dutschman, E. A. Gullen, M. Telpoukhovskaia, Y. C. Cheng, A. D. Hamilton, *Bioorg. Med. Chem. Lett.* **2010**, *20*, 2137–2139.
[33] M. Mourer, N. Psychogios, G. Laumond, A. M. Aubertin, J. B. Regnouf-de-Vains, *Bioorg. Med. Chem.* **2010**, *18*, 36–45.
[34] A. I. Vovk, V. I. Kalchenko, S. A. Cherenok, V. P. Kukhar, O. V. Muzychka, M. O. Lozynsky, *Org. Biomol. Chem.* **2004**, *2*, 3162–3166.
[35] S. Cherenok, A. Vovk, I. Muravyova, A. Shivanyuk, V. Kukhar, J. Lipkowski, V. Kalchenko, *Org. Lett.* **2006**, *8*, 549–552.
[36] A. I. Vovk, L. A. Kononets, V. Y. Tanchuk, A. B. Drapailo, V. I. Kalchenko, V. P. Kukhar, *J. Inclusion Phenom. Macrocyclic Chem.* **2010**, *66*, 271–277.
[37] V. Martos, S. C. Bell, E. Santos, E. Y. Isacoff, D. Trauner, J. De Mendoza, *PNAS* **2009**, *106*, 10482–10486.
[38] M. G. Chini, S. Terracciano, R. Riccio, G. Bifulco, R. Ciao, C. Gaeta, F. Troisi, P. Neri, *Org. Lett.* **2010**, *12*, 5382–5385.
[39] R. P. M. Dings, M. C. Miller, I. Nesmelova, L. Astorgues-Xerri, N. Kumar, M. Serova, X. Chen, E. Raymond, T. R. Hoye, K. H. Mayo, *J. Med. Chem.* **2012**, *55*, 5121–5129.
[40] E. Raymond, *Eur. J. Cancer* **2014**, *50*, 2463–2477.
[41] S. O. Cherenok, O. A. Yushchenko, V. Y. Tanchuk, I. M. Mischenko, N. V. Samus, O. V. Ruban, Y. I. Matvieiev, J. A. Karpenko, V. P. Kukhar, A. I. Vovk, V. I. Kalchenko, *Arkivoc* **2012**, *4*, 278–298.
[42] O. Kobzar, Y. Shulha, V. Buldenko, A. Drapailo, V. Kalchenko, A. Vovk, *Ukrainica Bioorg. Acta* **2022**, *17*, 86–91.
[43] V. V. Trush, S. O. Cherenok, V. Y. Tanchuk, V. P. Kukhar, V. I. Kalchenko, A. I. Vovk, *Bioorg. Med. Chem. Lett.* **2013**, *23*, 5619–5623.

[44] V. M. Buldenko, V. V. Trush, O. L. Kobzar, A. B. Drapailo, V. I. Kalchenko, A. I. Vovk, *Bioorg. Med. Chem. Lett.* **2019**, *29*, 797–801.

[45] A. I. Vovk, L. A. Kononets, V. Y. Tanchuk, S. O. Cherenok, A. B. Drapailo, V. I. Kalchenko, V. P. Kukhar, *Bioorg. Med. Chem. Lett.* **2010**, *20*, 483–487.

[46] O. L. Kobzar, M. V. Shevchuk, A. N. Lyashenko, V. Y. Tanchuk, V. D. Romanenko, S. M. Kobelev, A. D. Averin, I. P. Beletskaya, A. I. Vovk, V. P. Kukhar, *Org. Biomol. Chem.* **2015**, *13*, 7437–7444.

[47] Z. Luo, Y. Zhao, C. Ma, Z. Li, X. Xu, L. Hu, N. Huang, H. He, *Arch. Pharm. (Weinheim)* **2015**, *348*, 206–213.

[48] Z. G. Luo, Y. Zhao, C. Ma, X. M. Xu, X. M. Zhang, N. Y. Huang, H. Q. He, *Chin. Chem. Lett.* **2014**, *25*, 737–740.

[49] K. A. Khadra, S. Mizyed, D. Marji, S. F. Haddad, M. Ashram, A. Foudeh, *Spectrochim. Acta A Mol. Biomol. Spectrosc.* **2015**, *136*, 1869–1874.

[50] S. Tommasone, C. Talotta, C. Gaeta, L. Margarucci, M. C. Monti, A. Casapullo, B. MacChi, S. P. Prete, A. Ladeiradearaujo, P. Neri, *Angew. Chem. - Int. Ed.* **2015**, *54*, 15405–15409.

[51] K. J. P. Rocha-Brito, E. M. B. Fonseca, B. G. de F. Oliveira, Â. de Fátima, C. V. Ferreira-Halder, *Bioorg. Chem.* **2020**, *100*, 103881.

[52] N. Humbert, L. Kovalenko, F. Saladini, A. Giannini, M. Pires, T. Botzanowski, S. Cherenok, C. Boudier, K. K. Sharma, E. Real, O. A. Zaporozhets, S. Cianférani, C. Seguin-Devaux, F. Poggialini, M. Botta, M. Zazzi, V. I. Kalchenko, M. Mori, Y. Mély, *ACS Infect. Dis.* **2020**, *6*, 687–702.

[53] J. P. Schneider, S. Tommasone, P. Della Sala, C. Gaeta, C. Talotta, C. Tarnus, P. Neri, A. Bodlenner, P. Compain, *Pharmaceuticals* **2020**, *13*, 366.

[54] S. Xia, Y. Jiang, X. Guo, Y. Wang, W. Xu, *J. Mol. Liq.* **2022**, *367*, 120398.

[55] D. Sbravati, A. Bonardi, S. Bua, A. Angeli, M. Ferraroni, A. Nocentini, A. Casnati, P. Gratteri, F. Sansone, C. T. Supuran, *Chem. A Eur. J.* **2022**, *28*, e202103527.

[56] M. M. Naseer, M. Ahmed, S. Hameed, *Chem. Biol. Drug Des.* **2017**, *89*, 243–256.

[57] S. Kamata, T. Oyama, K. Saito, A. Honda, Y. Yamamoto, K. Suda, R. Ishikawa, T. Itoh, Y. Watanabe, T. Shibata, K. Uchida, M. Suematsu, I. Ishii, *iScience* **2020**, *23*, 101727.

[58] H. E. Xu, M. H. Lambert, V. G. Montana, K. D. Plunket, L. B. Moore, J. L. Collins, J. A. Oplinger, S. A. Kliewer, J. Gampe, D. D. McKee, J. T. Moore, T. M. Willson, *PNAS* **2001**, *98*, 13919–13924.

[59] S. Kamata, T. Oyama, K. Saito, A. Honda, Y. Yamamoto, K. Suda, R. Ishikawa, T. Itoh, Y. Watanabe, T. Shibata, K. Uchida, M. Suematsu, I. Ishii, *iScience* **2020**, *23*, 101727.

[60] J. P. Overington, B. Al-Lazikani, A. L. Hopkins, *Nat. Rev. Drug Discov.* **2006**, *5*, 993–996.

[61] A. C. W. Pike, A. M. Brzozowski, R. E. Hubbard, T. Bonn, A. G. Thorsell, O. Engström, J. Ljunggren, J. Gustafsson, M. Carlquist, *EMBO J.* **1999**, *18*, 4608–4618.

[62] S. P. Williams, P. B. Sigler, *Nature* **1998**, *393*, 392–396.

[63] P. M. Matias, P. Donner, R. Coelho, M. Thomaz, C. Peixoto, S. Macedo, N. Otto, S. Joschko, P. Scholz, A. Wegg, S. Bäsler, M. Schäfer, U. Egner, M. A. Carrondo, *J. Biol. Chem.* **2000**, *275*, 26164–26171.

[64] K. P. De, J. Sus-Tran, *Protein Sci.* **2006**, *15*, 987–999.

[65] L. Shan, J. Vincent, S. J. Brunzelle, I. Dussault, M. Lin, I. Ianculescu, M. A. Sherman, B. M. Forman, E. J. Fernandez, *Mol. Cell* **2004**, *16*, 907–917.

[66] J. Osz, Y. Brélivet, C. Peluso-Iltis, V. Cura, S. Eiler, M. Ruff, W. Bourguet, N. Rochel, D. Moras, *PNAS* **2012**, *109*, E588–E594.

[67] S. Svensson, T. Östberg, M. Jacobsson, C. Norström, K. Stefansson, D. Hallén, I. C. Johansson, K. Zachrisson, D. Ogg, L. Jendeberg, *EMBO J.* **2003**, *22*, 4625–4633.

[68] C. Stehlin-Gaon, D. Willmann, D. Zeyer, S. Sanglier, A. Van Dorsselaer, J. P. Renaud, D. Moras, R. Schüle, *Nat. Struct. Mol. Biol.* **2003**, *10*, 820–825.

[69] C. Stehlin, J. M. Wurtz, A. Steinmetz, E. Greiner, R. Schüle, J. P. Renaud, *EMBO J.* **2001**, *20*, 5822–5831.

[70] V. Delfosse, T. Huet, D. Harrus, M. Granell, M. Bourguet, C. Gardia-Parège, B. Chiavarina, M. Grimaldi, S. Le Mével, P. Blanc, D. Huang, J. Gruszczyk, B. Demeneix, S. Cianférani, J. B. Fini, P. Balaguer, W. Bourguet, *PNAS* **2021**, *118*, e2020551118.

[71] R. E. Watkins, G. B. Wisely, L. B. Moore, J. L. Collins, M. H. Lambert, S. P. Williams, T. M. Willson, S. A. Kliewer, M. R. Redinbo, *Science* **2001**, *292*, 2329–2333.

[72] Y. Sato, N. Ramalanjaona, T. Huet, N. Potier, J. Osz, P. Antony, C. Peluso-Iltis, P. Poussin-Courmontagne, E. Ennifar, Y. Mély, A. Dejaegere, D. Moras, N. Rochel, *PLoS One* **2010**, *5*, e15119.

[73] W. Bourguet, V. Vivat, J. M. Wurtz, P. Chambon, H. Gronemeyer, D. Moras, *Mol. Cell* **2000**, *5*, 289–298.

[74] T. E. Speltz, C. G. Mayne, S. W. Fanning, Z. Siddiqui, E. Tajkhorshid, G. L. Greene, T. W. Moore, *Org. Biomol. Chem.* **2018**, *16*, 3702–3706.

[75] P. Y. Maximov, B. Abderrahman, S. W. Fanning, S. Sengupta, P. Fan, R. F. Curpan, D. M. Q. Rincon, J. A. Greenland, S. S. Rajan, G. L. Greene, V. Craig Jordan, *Mol. Pharmacol.* **2018**, *94*, 812–822.

[76] A. M. Leduc, J. O. Trent, J. L. Wittliff, K. S. Bramlett, S. L. Briggs, N. Y. Chirgadze, Y. Wang, T. P. Burris, A. F. Spatola, *PNAS* **2003**, *100*, 11273–11278.

[77] M. Calvaresi, S. Furini, C. Domene, A. Bottoni, F. Zerbetto, *ACS Nano* **2015**, *9*, 4827–4834.

[78] J. H. Morais-Cabral, Y. Zhou, R. MacKinnon, *Nature* **2001**, *414*, 37–42.

[79] L. G. Cuello, V. Jogini, D. M. Cortes, A. C. Pan, D. G. Gagnon, O. Dalmas, J. F. Cordero-Morales, S. Chakrapani, B. Roux, E. Perozo, *Nature* **2010**, *466*, 272–275.

[80] Y. J. Im, S. Raychaudhuri, W. A. Prinz, J. H. Hurley, *Nature* **2005**, *437*, 154–158.

[81] S. W. Cowan, M. E. Newcomer, T. A. Jones, *Proteins Struct. Funct. Bioinf.* **1990**, *8*, 44–61.

[82] H. L. Monaco, M. Rizzi, A. Coda, *Science* **1995**, *268*, 1039–1041.

[83] G. W. Han, J. Y. Lee, H. K. Song, C. Chang, K. Min, J. Moon, D. H. Shin, M. L. Kopka, M. R. Sawaya, H. S. Yuan, T. D. Kim, J. Choe, J. Lim, H. J. Moon, S. W. Suh, *J. Mol. Biol.* **2001**, *308*, 263–278.

[84] S. Tassin-Moindrot, A. Caille, J. P. Douliez, D. Marion, F. Vovelle, *Eur. J. Biochem.* **2000**, *267*, 1117–1124.

[85] M. E. Newcomer, *Structure* **1993**, *1*, 7–18.

[86] J. C. Sacchettini, J. l. Gordon, L. J. Banaszak, *J. Mol. Biol.* **1989**, *208*, 327–339.

[87] R. Huber, M. Schneider, I. Mayr, R. Müller, R. Deutzmann, F. Suter, H. Zuber, H. Falk, H. Kayser, *J. Mol. Biol.* **1987**, *198*, 499–513.

[88] J. Ghuman, P. A. Zunszain, I. Petitpas, A. A. Bhattacharya, M. Otagiri, S. Curry, *J. Mol. Biol.* **2005**, *353*, 38–52.

[89] I. Petitpas, A. A. Bhattacharya, S. Twine, M. East, S. Curry, *J. Biol. Chem.* **2001**, *276*, 22804–22809.

[90] J. L. Perry, M. R. Goldsmith, T. R. Williams, K. P. Radack, T. Christensen, J. Gorham, M. A. Pasquinelli, E. J. Toone, D. N. Beratan, J. D. Simon, *Photochem. Photobiol.* **2006**, *82*, 1365–1369.

[91] Y. Ali, N. M. Eltayeb, S. M. Salhimi, M. Taher, S. Abd Hamid, *J. Inclusion Phenom. Macrocyclic Chem.* **2022**, *102*, 873–880.

[92] I. R. Hardcastle, C. E. Arris, J. Bentley, F. T. Boyle, Y. Chen, N. J. Curtin, J. A. Endicott, A. E. Gibson, B. T. Golding, R. J. Griffin, P. Jewsbury, J. Menyerol, V. Mesguiche, D. R. Newell, M. E. M. Noble, D. J. Pratt, L. Z. Wang, H. J. Whitfield, *J. Med. Chem.* **2004**, *47*, 3710–3722.

[93] W. F. De Azevedo, S. Leclerc, L. Meijer, L. Havlicek, M. Strnad, S. H. Kim, *Eur. J. Biochem.* **1997**, *243*, 518–526.

[94] L. Ulfo, P. E. Costantini, M. Di Giosia, A. Danielli, M. Calvaresi, *Pharmaceutics* **2022**, *14*, 241.

[95] E. R. Wood, A. T. Truesdale, O. B. McDonald, D. Yuan, A. Hassell, S. H. Dickerson, C. Ellis, C. Pennisi, E. Horne, K. Lackey, K. J. Alligood, D. W. Rusnak, T. M. Gilmer, L. Shewchuk, *Cancer Res.* **2004**, *64*, 6652–6659.

[96] Y. Yosaatmadja, C. J. Squire, M. McKeage, J. U. Flanagan, **2014**, https://doi.org/10.2210/pdb4wkq/pdb.

[97] Z. Zhao, L. Xie, P. E. Bourne, *J. Chem. Inf. Model.* **2019**, *59*, 453–462.

[98] M. R. Sawaya, J. Kraut, *Biochemistry* **1997**, *36*, 586–603.

[99] A. Gangjee, A. P. Vidwans, A. Vasudevan, S. F. Queener, R. L. Kisliuk, V. Cody, R. Li, N. Galitsky, J. R. Luft, W. Pangborn, *J. Med. Chem.* **1998**, *41*, 3426–3434.

[100] J. F. Davies, T. J. Delcamp, N. J. Prendergast, V. A. Ashford, J. H. Freisheim, J. Kraut, *Biochemistry* **1990**, *29*, 9467–9479.

[101] P. L. Boyer, S. J. Smith, X. Z. Zhao, K. Das, K. Gruber, E. Arnold, T. R. Burke, S. H. Hughes, *J. Virol.* **2018**, *92*, e02203–17.

[102] J. Ren, R. M. Esnouf, A. L. Hopkins, J. Warren, J. Balzarini, D. I. Stuart, D. K. Stammers, *Biochemistry* **1998**, *37*, 14394–14403.

[103] C. H. Shen, Y. F. Wang, A. Y. Kovalevsky, R. W. Harrison, I. T. Weber, *FEBS J.* **2010**, *277*, 3699–3714.

[104] H. Jhoti, O. M. P. Singh, M. P. Weir, R. Cooke, P. Murray-Rust, A. Wonacott, *Biochemistry* **1994**, *33*, 8417–8427.

[105] Y. Zhang, A. A. Simpson, R. M. Ledford, C. M. Bator, S. Chakravarty, G. A. Skochko, T. M. Demenczuk, A. Watanyar, D. C. Pevear, M. G. Rossmann, *J. Virol.* **2004**, *78*, 11061–11069.

[106] J. Badger, I. Minor, M. A. Oliveira, T. J. Smith, M. G. Rossmann, *Proteins Struct. Funct. Bioinf.* **1989**, *6*, 1–19.

[107] A. Daina, O. Michielin, V. Zoete, *Nucl. Acids Res.* **2019**, *47*, 357–354.

[108] Y. Zhao, D. G. Truhlar, *Theor. Chem. Acc.* **2008**, *120*, 215.

[109] Gaussian 16, Revision C.01, M. J. Frisch, G. W. Trucks, H. B. Schlegel, G. E. Scuseria, M. A. Robb, J. R. Cheeseman, G. Scalmani, V. Barone, G. A. Petersson, H. Nakatsuji, X. Li, M. Caricato, A. V. Marenich, J. Bloino, B. G. Janesko, R. Gomperts, B. Mennucci, H. P. Hratchian, J. V. Ortiz, A. F. Izmaylov, J. L. Sonnenberg, D. Williams-Young, F. Ding, F. Lipparini, F. Egidi, J. Goings, B. Peng, A. Petrone, T. Henderson, D. Ranasinghe, V. G. Zakrzewski, J. Gao, N. Rega, G. Zheng, W. Liang, M. Hada, M. Ehara, K. Toyota, R. Fukuda, J. Hasegawa, M. Ishida, T. Nakajima, Y. Honda, O. Kitao, H. Nakai, T. Vreven, K. Throssell, J. A. Montgomery, Jr., J. E. Peralta, F. Ogliaro, M. J. Bearpark, J. J. Heyd, E. N. Brothers, K. N. Kudin, V. N. Staroverov, T. A. Keith, R. Kobayashi, J. Normand, K. Raghavachari, A. P. Rendell, J. C. Burant, S. S. Iyengar, J. Tomasi, M. Cossi, J. M. Millam, M. Klene, C. Adamo, R. Cammi, J. W. Ochterski, R. L. Martin, K. Morokuma, O. Farkas, J. B. Foresman, and D. J. Fox, Gaussian, Inc., Wallingford CT, **2016**.

[110] J. Tomasi, B. Mennucci, R. Cammi, *Chem. Rev.* **2005**, *105*, 2999–3094.

[111] J. Wang, R. M. Wolf, J. W. Caldwell, P. A. Kollman, D. A. Case, *J. Comput. Chem.* **2004**, *25*, 1157–1174.

[112] C. I. Bayly, P. Cieplak, W. D. Cornell, P. A. Kollman, *J. Phys. Chem.* **1993**, *97*, 10269–10280.

[113] Z. Gao, H. Li, H. Zhang, X. Liu, L. Kang, X. Luo, W. Zhu, K. Chen, X. Wang, H. Jiang, *BMC Bioinf.* **2008**, *9*, 1–7.

[114] D. Schneidman-Duhovny, Y. Inbar, V. Polak, M. Shatsky, I. Halperin, H. Benyamini, A. Barzilai, O. Dror, N. Haspel, R. Nussinov, H. J. Wolfson, *Proteins Struct. Funct. Bioinf.* **2003**, *52*, 107–112.

[115] N. Andrusier, R. Nussinov, H. J. Wolfson, *Proteins Struct. Funct. Bioinf.* **2007**, *69*, 139–159.

[116] A. Marconi, G. Giugliano, M. Di Giosia, T. D. Marforio, M. Trivini, E. Turrini, C. Fimognari, F. Zerbetto, E. J. Mattioli, M. Calvaresi, *Pharmaceutics* **2023**, *15*, 919.

[117] A. Marconi, J. Mattioli, F. Ingargiola, G. Giugliano, D. Marforio, L. Prodi, M. Di Giosia, M. Calvaresi, *Molecules* **2023**, *28*, 2348.

[118] E. J. Mattioli, L. Ulfo, A. Marconi, V. Pellicioni, P. E. Costantini, T. D. Marforio, M. Di Giosia, A. Danielli, C. Fimognari, E. Turrini, M. Calvaresi, *Biomolecules* **2023**, *13*, 68.

[119] K. Malarz, J. Korzuch, T. D. Marforio, K. Balin, M. Calvaresi, A. Mrozek-Wilczkiewicz, R. Musiol, M. Serda, *Int. J. Nanomed.* **2023**, *18*, 1709–1724.

[120] A. Cantelli, M. Malferrari, E. J. Mattioli, A. Marconi, G. Mirra, A. Soldà, T. D. Marforio, F. Zerbetto, S. Rapino, M. Di Giosia, M. Calvaresi, *Nanomaterials* **2022**, *12*, 3501.

[121] M. Calvaresi, F. Zerbetto, *ACS Nano* **2010**, *4*, 2283–2299.

[122] M. di Giosia, F. Valle, A. Cantelli, A. Bottoni, F. Zerbetto, M. Calvaresi, *Materials* **2018**, *11*, 691.

[123] M. Di Giosia, A. Soldà, M. Seeger, A. Cantelli, F. Arnesano, M. I. Nardella, V. Mangini, F. Valle, M. Montalti, F. Zerbetto, S. Rapino, M. Calvaresi, V. Ntziachristos, *Adv. Funct. Mater.* **2021**, *31*, 2101527.

[124] M. Calvaresi, F. Zerbetto, *J. Chem. Inf. Model.* **2011**, *51*, 1882–1896.

[125] T. D. Marforio, E. J. Mattioli, F. Zerbetto, M. Calvaresi, *Nanomaterials* **2023**, *13*, 1770.

[126] M. Di Giosia, F. Valle, A. Cantelli, A. Bottoni, F. Zerbetto, E. Fasoli, M. Calvaresi, *Carbon N Y* **2019**, *147*, 70–82.

[127] M. Di Giosia, T. D. Marforio, A. Cantelli, F. Valle, F. Zerbetto, Q. Su, H. Wang, M. Calvaresi, *J. Colloid Interface Sci.* **2020**, *571*, 174–184.

[128] C. Zhang, G. Vasmatzis, J. L. Cornette, C. DeLisi, *J. Mol. Biol.* **1997**, *267*, 707–726.

[129] C. L. Kingsford, B. Chazelle, M. Singh, *Bioinformatics* **2005**, *21*, 1028–1039.

[130] J. A. Maier, C. Martinez, K. Kasavajhala, L. Wickstrom, K. E. Hauser, C. Simmerling, *J. Chem. Theory Comput.* **2015**, *11*, 3696–3713.

[131] D.A. Case, R.M. Betz, D.S. Cerutti, T.E. Cheatham, III, T.A. Darden, R.E. Duke, T.J. Giese, H. Gohlke, A.W. Goetz, N. Homeyer, S. Izadi, P. Janowski, J. Kaus, A. Kovalenko, T.S. Lee, S. LeGrand, P. Li, C. Lin, T. Luchko, R. Luo, B. Madej, D. Mermelstein, K.M. Merz, G. Monard, H. Nguyen, H.T. Nguyen, I. Omelyan, A. Onufriev, D.R. Roe, A. Roitberg, C. Sagui, C.L. Simmerling, W.M. Botello-Smith, J. Swails, R.C. Walker, J. Wang, R.M. Wolf, X. Wu, L. Xiao and P.A. Kollman, AMBER16 **2016**, University of California, San Francisco.

[132] A. V. Onufriev, *Annu. Rev. Biophys.* **2019**, *48*, 275–96

[133] B. R. Miller, T. D. McGee, J. M. Swails, N. Homeyer, H. Gohlke, A. E. Roitberg, *J. Chem. Theory Comput.* **2012**, *8*, 3314–3321.

[134] A. Bartocci, N. Gillet, T. Jiang, F. Szczepaniak, E. Dumont, *J. Phys. Chem. B* **2020**, *124*, 11371–11378.

[135] A. Bartocci, G. Pereira, M. Cecchini, E. Dumont, *J. Chem. Inf. Model.* **2022**, *62*, 6739–6748.

[136] A. Bartocci, E. Dumont, *Phys. Chem. Chem. Phys.* **2023**, *25*, 18067–18074.

[137] R. J. Flood, L. Cerofolini, M. Fragai, P. B. Crowley, *Biomacromolecules* **2024**, *25*, 1303–1309.

[138] E. Chovancova, A. Pavelka, P. Benes, O. Strnad, J. Brezovsky, B. Kozlikova, A. Gora, V. Sustr, M. Klvana, P. Medek, L. Biedermannova, J. Sochor, J. Damborsky, *PLoS Comput. Biol.* **2012**, *8*, e1002708.

[139] O. Vavra, J. Filipovic, J. Plhak, D. Bednar, S. M. Marques, J. Brezovsky, L. Stourac, J. Matyska, J. Damborsky, *Bioinformatics* **2019**, *35*, 4986–4993.